Chemical Science

ROYAL SOCIETY OF CHEMISTRY

EDGE ARTICLE

View Article Online
View Journal

Cite this: DOI: 10.1039/d5sc05918f

All publication charges for this article have been paid for by the Royal Society of Chemistry

Interplay between diradical character, aromaticity and conductance in oligothiophenes

Louis Van Nyvel, [a] Irene Casademont-Reig, [ab] Jochen Eeckhoudt, [a] Sergio Moles Quintero, [a] Frank De Proft, [a] Paul Geerlings [a] and Mercedes Alonso *[a]

The fundamental relationships of the diradical character–aromaticity–conductance triangle are elucidated across a diverse set of oligothiophenes capable of adopting both aromatic and quinoidal structures. The electronic ground-state was determined using open-shell/closed-shell and singlet–triplet adiabatic energy gaps, while the diradical character (y_0) was quantified using Yamaguchi's approach. All oligomers exhibit a singlet ground state, with only 13 being open-shell with non-zero diradical character. A strong correlation between the multicenter index of the central thiophene ring(s) and y_0 indicates that the diradical character and aromaticity vertices are intrinsically linked: modulation of one invariably impacts the other. The diradical character–conductance relationship reveals two competing effects: while higher y_0 generally enhances conductance, this trend is counterbalanced by length-dependent attenuation, leading to near-zero conductance in sufficiently long oligomers (~20 Å). Additionally, systems with $y_0 \approx 1$ exhibit reduced conductance regardless of molecular length. Conductance also correlates with local aromaticity: annulated rings that most strongly disrupt the aromaticity of the backbone thiophene units yield higher conductance compared to parent structures. In terms of the linear aromaticity, approximately 70% of local transmission plots could be identified through pathways derived from the AV_{min} index and delocalization indices, underscoring their predictive value for local charge transport behavior. This study extends the traditional diradical–aromaticity–conductance triangle by incorporating the electronic ground-state structure as a fourth vertex and distinguishing between local and global aromaticity–conductance relationships. The resulting framework provides deeper insight into the shared electronic origins of key molecular properties and their influence on charge transport.

Received 5th August 2025
Accepted 2nd December 2025

DOI: 10.1039/d5sc05918f

rsc.li/chemical-science

Introduction

Since the pioneering work of Aviram and Ratner,[1] molecular electronics has emerged over the past decades as an increasingly important interdisciplinary field.[2–4] A central aspect of the field is the fabrication of molecular junctions that enable the probing and manipulation of charge transport through individual molecules.[5] A variety of experimental techniques for constructing such single–molecule junctions has been engineered,[6–8] alongside the development of theoretical methods based on Green's function theory allowing the investigation of single-molecule transport properties under non-equilibrium conditions.[9,10] These methods are crucial for rationalizing the complicated experimental observations and guiding the design of novel building blocks for molecular-scale electronic applications.[11,12]

A key aspect of theoretical developments is the interpretation of charge transport data in terms of well-established chemical concepts, which can then be leveraged in the molecular design process. Aromaticity is among the most frequently addressed concepts in this context (*vide infra*). Similarly, the relationship between the diradical character of a single molecule and its conductance has attracted considerable attention in recent years.[13] Although neither diradical character nor aromaticity is directly accessible through experiment, correlations with experimentally measurable quantities have been proposed.[14–16] In particular, Nakano *et al.* have established a direct link between diradical character and experimentally measurable quantities,[14] while aromaticity has a long-standing history of indirect experimental probing.[17–20]

A higher diradical character in a molecule has been proposed to enhance conductance, particularly when the contacts are positioned on the carbon atoms constituting the radical centers.[21] This relationship was emphasized when highlighting the significance of the diradical resonance structures within the overall resonance hybrid of the molecule.[22] These insights offer a design strategy for tuning molecular

[a]Department of General Chemistry (ALGC), Vrije Universiteit Brussel (VUB), Pleinlaan 2, 1050 Brussels, Belgium. E-mail: mercedes.alonso.giner@vub.be
[b]Donostia International Physics Center (DIPC), 20018 Donostia, Euskadi, Spain

conductance by modulating the diradical character. In particular, conductance can be enhanced by maximizing the contribution of resonance structures in which the radical centers align with the contact positions.[21,23,24]

A recent perspective underscores the potential of radical single–molecule junctions, proposing design principles for the synthesis of stable radicals relevant to nanoscale electronic devices.[25] Nevertheless, single-molecule measurements involving radicals remain relatively scarce primarily due to their limited stability under the experimental conditions. In parallel, considerable attention has been devoted to understanding how conductance varies with the length of molecular wires. Anti-ohmic behavior (*i.e.,* conductance increases with molecular length) has been proposed,[26–30] among others, by Stuyver *et al.* on the basis of theoretical studies invoking the role of diradical character.[23] However, these predictions have been challenged by Mandado and co-workers on the grounds that single-determinant methods are inadequate for describing diradical species.[31] More recently, both theoretical and experimental studies have put forward cases consistent with anti-ohmic effects, where conductance reaches a maximum at a specific number of monomer units, followed by a decrease as the oligomer length increases further.[26–28] While the literature sheds light on the relationship between diradical character and single-molecule conductance, a unified framework that also incorporates the effects of aromaticity and molecular wire length has yet to be established.

The relationship between conductance and aromaticity remains controversial. Breslow and co-workers provided experimental evidence suggesting that the aromaticity of individual five-membered rings correlates negatively with molecular conductance.[32] Accordingly, antiaromatic systems are expected to conduct better than nonaromatic ones, which in turn are anticipated to exhibit higher conductance than aromatic compounds.[33,34] However, this trend does not hold universally, as we demonstrated for expanded porphyrins, which serve as an excellent platform for exploring the relationship between aromaticity and molecular properties owing to their structural flexibility and rich redox chemistry.[16,35,36] Connecting the electrodes along the longitudinal axis of the macrocycle enables constructive or destructive quantum interference effects depending on the aromatic or antiaromatic character of the system.[35,37] Similarly, for a diverse set of polycyclic compounds a positive relationship was observed between the aromaticity of the molecular core and the zero-bias conductance for a given connectivity to the metallic electrodes.[38]

A fundamental aspect in understanding the aromaticity–conductance relationship is the distinction between global aromaticity, attributed to the entire molecular system, and local aromaticity, linked to specific subunits of the molecular framework. The inverse correlation between aromaticity and conductance observed in 2014 involves single monocyclic systems, such as thiophene, furan, and cyclopentadiene and thus represents a case centered on global aromaticity.[32] In contrast, our extensive investigations on expanded porphyrins and polycyclic aromatic hydrocarbons consider not only their global aromaticity, but also the local aromaticity of their individual five- and six-membered rings.[35,37–43] The local aromaticity features naturally lead to the identification of the most conjugated pathway within these macrocyclic and polycyclic compounds, serving as a roadmap for the electron current and the overall conductance.[37,38,41,44]

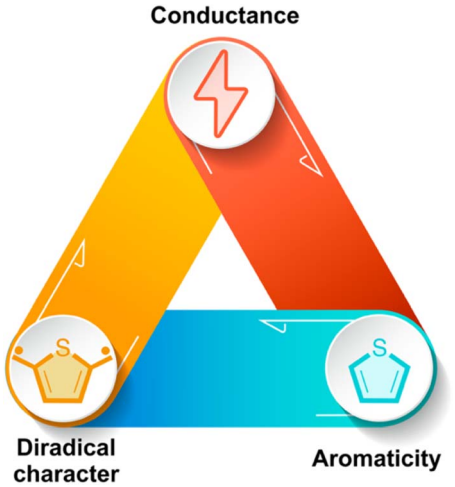

Fig. 1 Schematic overview of the interplay between diradical character, aromaticity, and conductance examined in this work.

Linking the theoretical concepts of diradical character and aromaticity to an experimentally accessible quantity like conductance, requires a clear understanding of how these two concepts are connected. In other words, it calls for elucidating the interplay between diradical character and aromaticity. This study aims to further develop this conceptual framework by examining the triangular relationship between conductance, diradical character, and aromaticity, both global and local, as illustrated in Fig. 1. To this end, a comprehensive investigation employing a common testbed is undertaken, offering a systematic approach to explore the three key relationships, depicted as the sides of the triangle, by first analyzing its vertices.

Research strategy

Our approach begins with a detailed investigation of the electronic structure of the selected compounds, providing the foundation for evaluating both diradical character and various aromaticity descriptors, the first two vertices of the triangle, and their interrelationship, which constitutes one of its sides. Subsequently, conductance, the third vertex, is examined. This stepwise approach enables a complete disentangling of the triangle, ultimately shedding light on the remaining two connections (conductance–diradical character and conductance–aromaticity) which may themselves be intertwined. The outcome of this investigation might provide a conceptual framework to facilitate the design of highly conducting molecular wires.

We examine a series of linear oligothiophenes with varying length and distinctive structural features (Scheme 1A) as they constitute an ideal testbed for probing the interplay between aromaticity, diradical character, and single-molecule

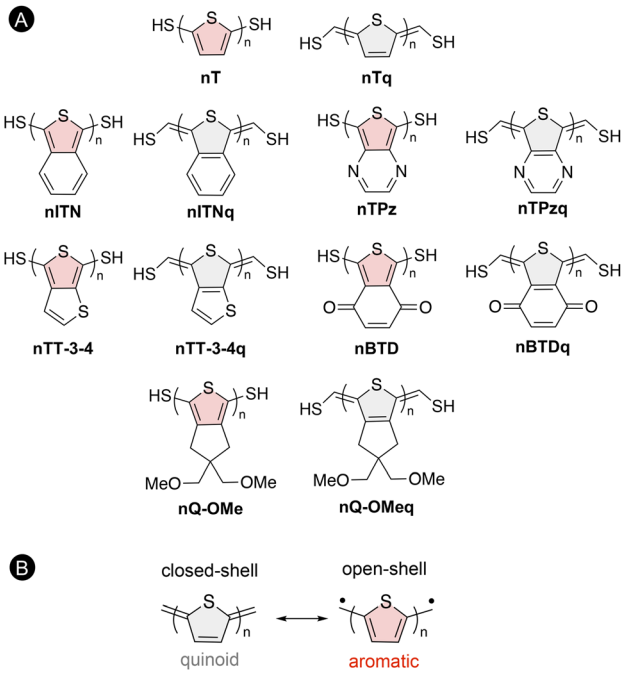

Scheme 1 (A) Oligothiophenes selected to assess the interplay between diradical character, aromaticity, and conductance. The quinoidal oligothiophenes are indicated by the suffix "**q**". The oligomer chain *n* varies from one to six monomer units. (B) Quinoidal and aromatic resonance structures proposed for the singlet ground state of quinoidal oligothiophenes.

conductance. Owing to their tunable π-conjugation, favorable electronic properties, and synthetic accessibility, oligothiophenes are among the most important π-conjugated frameworks for elucidating structure-charge transport relationships from both experimental and computational perspectives.[45–56] While an exponential decrease in conductance with increasing molecular length (ohmic behavior) has been observed in several oligothiophene wires consistent with a tunnelling conduction mechanism,[47,48,57–61] multiple studies have reported significant deviations from this expected behavior. These have been linked to several factors, including the conjugation pattern, molecular conformation, and the influence of water on the gold–molecule interface.[48,50,52–54,57] In fact, the length dependence of conductance in oligothiophenes has become a focal point in molecular electronics, offering valuable insights into how the degree of π-conjugation affects charge transport at the single-molecule level. Notably, Xu *et al.* found that the longer oligothiophene with 4 repeating units exhibited higher conductance than the shorter, 3-unit analogue. A similar trend was recently observed by Jiang *et al.* for cationic oligophenylene-bridged bis(triarylamine) systems, which displayed a reversed exponential conductance decay for $n \leq 3$.[26] In this context, our set of oligothiophenes provides a platform to explore ohmic *versus* anti-ohmic trends, alongside a detailed investigation of their aromatic and diradical character.

The selected oligothiophenes are functionalized with thiol anchoring groups at both terminal positions to enable stable Au–S linkages, thereby enhancing the stability of the molecular junction.[2,45,56] Depending on the terminal groups, –SH or =CH–SH, the molecular building blocks are categorized into the "aromatic" and the "quinoidal" series, respectively (the latter indicated by the suffix "**q**"). As depicted in Scheme 1, the monomer units in the aromatic oligomers are formally connected by single bonds, whereas in the quinoidal series by formal double bonds. Appealingly, the ground state of quinoidal oligothiophenes is best described as a balance of quinoidal closed-shell and aromatic open-shell resonance structures (Scheme 1B).[62–64] The preference for either bonding pattern is governed by the number of repeat units *n*, which in turn leads to significant differences in the electronic structure of the resulting oligothiophenes, strongly impacting their optical, magnetic, and charge transport properties.[65–69] An illustrative example of the quinoidal-to-aromatic transformation is provided by tetracyano quinoidal oligothiophenes (**Q*n***) which display a marked evolution in the electronic structure as a function of chain length, as shown in Scheme S1 of the SI.[62,63,66]

In this context, the choice of linear oligothiophenes offers a significant advantage for analyzing local and global aromaticity, compared to macrocycles like expanded porphyrins.[41,44] Their linear chain rather than a cyclic π-conjugated architecture simplifies the aromaticity analysis.[70]

Beyond chain length, the properties of both aromatic and quinoidal oligothiophenes are influenced by the incorporation of substituents, heteroatoms, and annulated five- and six-membered rings, such as benzene, pyrazine, thiophene, benzoquinone, and cyclopentane, onto the parent thiophene core, thereby providing a diverse testbed (Scheme 1) for evaluating the impact of structural modifications on their electronic and transport characteristics.[63,66,68,71,72] These compounds comprise synthetically accessible units[73–80] carefully selected from previous studies.[62,71]

Computational methodology

Ground-state multiplicity, energy gaps, and diradical character

To determine the ground state multiplicity of the selected oligothiophenes the closed-shell (CSS) and open-shell singlet (OSS) structures as well as the triplet (T) states were optimized and fully characterized at the (U)CAM-B3LYP/cc-pVTZ level of theory using the Gaussian 16 software.[81–84] The choice of the CAM-B3LYP[81] functional was guided by both literature studies[85–88] and in-house benchmark calculations, which evaluated its performance for the ***n*T** series (see SI) against B3LYP[89,90] and M06-2X.[91] While B3LYP provided frontier orbital energies in good agreement with the experimental data reported by Capozzi,[52] recent studies have demonstrated that range-separated hybrids like CAM-B3LYP provide a more reliable framework for evaluating aromaticity.[44,92,93] Given the central role of aromaticity in this work, CAM-B3LYP was selected to mitigate the impact of the delocalization error on the aromaticity descriptors.[94,95] No planarity constraints were applied in our calculations. To quantify deviations from planarity in all oligothiophenes, the average dihedral angle

between the neighboring thiophene units were computed using the Mercury program.[97]

Frequency calculations were performed at the (U)CAM-B3LYP/cc-pVTZ level of theory to confirm that the optimized structures correspond to true minima on the potential energy surface and to obtain the zero-point vibrational energy (ZPVE). Unrestricted broken-symmetry DFT was applied to generate an open-shell singlet solution. Such an approach has been shown to provide reliable geometries and energies for singlet diradical states, including quinoidal oligothiophenes.[62,68,96]

From the optimized geometries, the open-/closed-shell ($\Delta E_{OS\text{-}CS}$) and the singlet–triplet (ΔE_{ST}) adiabatic energy gaps were determined. A negative $\Delta E_{OS\text{-}CS}$ value indicates that the lowest singlet state is an open-shell (OS) state with broken symmetry. The * notation is used for cases where the OS electronic structure converged to a closed-shell (CS) ground state. In the case of the singlet–triplet gap, a negative value denotes that the singlet state is energetically favored over the triplet.

The oligothiophenes' diradical character, evaluated at the optimized geometry of the lowest-energy singlet state, was determined using Yamaguchi's approach,[98–100] previously adopted in similar studies.[68,101] His expression is based on the occupation numbers (n_i) of the natural orbitals (NO).[102,103]

$$y_i = 1 - \frac{2T_i}{1 + T_i^2} \quad (1)$$

$$T_i = \frac{n_{HONO-i} - n_{LUNO+i}}{2} \quad (2)$$

The diradical character (y_0), obtained *via* eqn (1) and (2) with $i = 0$, ranges between 0 (closed-shell) and 1 (pure diradical).[104] Two consecutive single-point calculations were performed in which the level of theory was increased between the two steps to ensure SCF convergence. For the first step, (U)HF/6-31G(d) was employed. Since the y_0 values are known to depend on the selected level of theory,[103] we performed benchmark calculations on the parent quinoid ***n*Tq** series using unrestricted PBE0 (ref. 105) and PBE0-DH[106] single reference methods and CASSCF(6,6) and CASSCF(12,12) multireference methods[107] in combination with the 6-31G(d) basis set[108–111] to identify the most suitable method for the second step. Based on this benchmark, the double-hybrid UPBE0-DH was selected as the second level of theory due to its good balance between accuracy and computational cost (Fig. S3 and Table S10).

Local and linear aromaticity descriptors

Once the ground-state multiplicity was established, the delocalization indices (DIs) as well as the local and linear aromaticity were evaluated. The term local aromaticity refers to the extent of π-electron delocalization within the individual rings that form the molecule, providing insight into the intrinsic aromatic character of each subunit. In contrast, linear aromaticity quantifies the delocalization along an open conjugated circuit, directly related to the transmission path in single-molecule conductance calculations.[38] This concept will be referred to as the linear aromatic pathway (LAP).

A variety of local aromaticity indices were used, all of which are well established in literature.[112] The definitions and computational details of these aromaticity indices are provided in the SI. These descriptors include the delocalization index (DI),[113,114] the harmonic oscillator model of aromaticity (HOMA),[115] aromatic fluctuation index (FLU),[116] multicenter index (MCI),[117] I_{ring},[118,119] AV1245 index,[120] and AV_{min}.[44,120] Among these indices, MCI has emerged as the most accurate index in several tests carefully designed to assess the performance of aromaticity descriptors in organic and inorganic species.[121,122] The most conjugated pathway was identified by the highest AV_{min} value,[38,39,44] as calculated using the ESI-3D program.[123,†] For the evaluation of the structural and electronic indices, we adopted an atomic partitioning based on the quantum theory of atoms in molecules (QTAIM), as implemented in the AIMAll software.[124]

An important role is played by a tailored version of the BLA index, introduced by Ponce *et al.* to assess the degree of quinoidization/aromatization of the conjugated backbone.[62] The quinoidization/aromatization index (QAI) can be easily quantified based on selected C–C bond distances (eqn (3)), where α, α′, β, and β′, denote distinct carbon atoms within the thiophene ring (Scheme 2). Aromatic rings display a positive QAI value, whereas a quinoidal one is characterized by a negative QAI.

$$QAI = r_{\beta\beta'} - \frac{r_{\alpha\beta} + r_{\alpha'\beta'}}{2} \quad (3)$$

Transmission spectra and local transmission plots

The conductance ($G(E)$) at a given energy level (usually the Fermi level) is obtained from the transmission ($T(E)$) using the Landauer formula:[21,125,126]

$$G(E) = \frac{2e^2}{h} T(E) \quad (4)$$

These calculations were carried out combining the non-equilibrium Green's functions (NEGF) approach with density functional theory (DFT)[21,31] at the (U)PBE/LanL2DZ level of theory,[127–129] as implemented in the Artaios code.[130,131] Gold(111) surfaces were selected as electrodes and thiol groups as anchor units to connect the oligothiophenes to the metallic contacts. Thiol linkers were chosen as anchoring groups due to its high

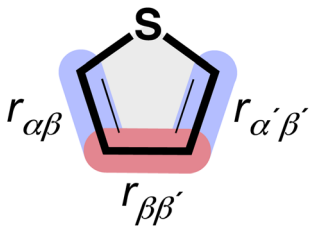

Scheme 2 Bond distances employed to evaluate the QAI index in oligothiophenes.

binding energy and high probability of junction formation, further supported by previous conductance measurements on thiol-terminated oligothiophenes.[4,26,59,132] Following the methodology outlined in our previous studies on single-molecule conductance,[21,35,38] the thiol's hydrogen atoms were removed and Au_9 clusters were attached. Fcc-hollow sites were selected as adsorption sites, and the Au–S distance was set to 2.48 Å. Besides the transmission spectra, local transmission plots (LTPs) were computed with the Artaios code.[133] To visualize preferential conduction pathways, through-bond transmission plots were generated using a threshold of the maximum atom–atom transmission at 20% with the POV-Ray software.[134] The blue arrow indicated current flow from left to right, while red arrows represent current flow following the opposite direction.

Results and discussion

Electronic ground states and diradical character (vertex 1)

As shown in Table 1, the ***n*T** structures exhibit a closed-shell ground-state across all oligomer lengths. Furthermore, the ΔE_{ST} values are all negative, consistently favoring a singlet ground state over the triplet. In contrast, for the quinoidal series (***n*Tq**), only the monomer and dimer display a closed-shell ground state. From the trimer (**3Tq**) onward, all oligomers prefer an open-shell singlet configuration. Moreover, their singlet–triplet gap decreases progressively with increasing chain length, yet remains negative, indicating that the open-shell singlet state remains more stable than the corresponding triplet state.

Regarding the effect of distinct annulated rings, the aromatic families depicted in Scheme 1 all adopt a closed-shell singlet ground state (Table S1). However, their singlet–triplet gaps are reduced compared to those of the parent ***n*T** series, as observed for the pyrazine (***n*TPz**), benzene (***n*ITN**), and thiophene (***n*TT-3-4**) derivatives (Fig. 2A). Interestingly, an increase in the ΔE_{ST} relative to the parent ***n*T** compounds is only observed when a saturated bis(methoxy)cyclopentane ring (***n*Q-OMe**) or benzoquinone unit (***n*BTD**) is fused to the thiophene core. For the quinoidal series (Fig. 2C), all systems exhibit a negative ΔE_{ST} indicating a preference for a singlet ground state (Table S1). As the oligomer length increases, a gradual stabilization of the lowest-lying triplet state is observed across all series. Within the annulated series, the incorporation of the benzoquinone unit (***n*BTDq**) leads to a faster reduction in the singlet–triplet energy gap compared to the parent ***n*Tq** series, whereas the 1,1-bis(methoxy)cyclopentane unit (***n*Q-OMeq**) produces no significant change, following a ΔE_{ST} evolution similar to that of the parent series.

Nevertheless, both series converge towards small ΔE_{ST} values in the pentamer and hexamer, approaching those reported for **5Tq** and **6Tq** in Table 1. These small ΔE_{ST} values suggest an equilibrium between the singlet and triplet states in the longer oligomers of ***n*Tq**, ***n*BTDq**, and ***n*Q-OMeq**, consistent with both experimental and theoretical observations reported for a related quinoidal oligothiophene bearing bis(butoxymethyl)cyclopentane groups and end-capped with dicyanomethylene units.[62] The remaining quinoidal series with aromatic annulated rings (***n*TPzq**, ***n*ITNq**, and ***n*TT-3-4q**) display significantly more negative ΔE_{ST} values from the monomer to the hexamer and consistently exhibit a closed-shell singlet ground state. This behavior may be attributed to the aromatic character of the annulated rings, as a transition to an open-shell configuration would result in the loss of aromatic stabilization. Notably, the pyrazine-fused system (***n*TPzq**) exerts the strongest influence on the singlet–triplet energy difference, followed by the benzene- (***n*ITNq**) and thiophene-annulated (***n*TT-3-4q**) derivatives, which exhibit smaller ΔE_{ST} values. Remarkably, this order is reversed in the corresponding aromatic series, where the pyrazine ring yields the smallest ΔE_{ST} across all oligomer lengths. Recent publications by Ie and co-workers have demonstrated the practical applications of π-extended quinoidal oligothiophenes, showing that the incorporation of fused aromatic rings such as pyrazine into the backbone stabilizes the quinoidal structure and enables the synthesis of increasingly longer conjugated systems. Owing to the enhanced quinoidal contribution to the ground state in the largest oligomers, these compounds exhibit absorption in the near-infrared (NIR) region, which in turn has enabled the evaluation of their performance in both organic phototransistors and organic solar cells.[135–137]

Overall, all structures in the aromatic series exhibit a closed-shell singlet ground state. Among the quinoidal oligothiophenes, only 13 structures (**3–6Tq**, **2–6BTDq**, and **3-6Q-OMeq**) display an open-shell singlet ground state, while the remaining quinoidal structures retain a closed-shell configuration, likely stabilized by the annulation of an aromatic ring.

To gain further insight into the ground-state multiplicity of the oligothiophenes, exploratory spin-flip (SF) calculations were performed.[138–144] The SF-TD-DFT results reinforce our previous conclusions, as the vertical singlet–triplet energy gaps follow trends similar to those observed in the adiabatic ΔE_{ST} values (Tables S5–S9 and Fig. S1–S2). However, these findings should be interpreted with caution, as analysis of the $\langle S^2 \rangle$ values revealed significant spin contamination in most cases. This issue merits further investigation in a separate study, as it extends beyond the scope of the present work.

For the parent quinoidal oligothiophene series (***n*Tq**), y_0 begins to increase from the trimer onwards, reaching values close to 1 for the longest oligomer with six repeat units,

Table 1 Adiabatic energy differences between the open- and closed-shell singlet states ($\Delta E_{OS\text{-}CS}$), adiabatic singlet–triplet gaps (ΔE_{ST}), and the spin-squared expectation value $\langle S^2 \rangle$ for the open-shell singlet configurations of compounds **1–6T** and **1–6Tq**. Relative energies (in kcal mol^{-1}) evaluated at the (U)CAM-B3LYP/cc-pVTZ level of theory. An asterisk (*) indicates that the open-shell solution converged to the closed-shell singlet

	$\Delta E_{OS\text{-}CS}$	ΔE_{ST}	$\langle S^2 \rangle$		$\Delta E_{OS\text{-}CS}$	ΔE_{ST}	$\langle S^2 \rangle$
1T	*	−60.05	0.00	**1Tq**	*	−27.80	0.00
2T	*	−46.37	0.00	**2Tq**	*	−11.59	0.00
3T	*	−39.03	0.00	**3Tq**	−3.63	−1.56	0.92
4T	*	−35.96	0.00	**4Tq**	−10.00	−1.85	1.21
5T	*	−34.31	0.00	**5Tq**	−16.90	−0.78	1.22
6T	*	−33.43	0.00	**6Tq**	−24.33	−0.27	1.20

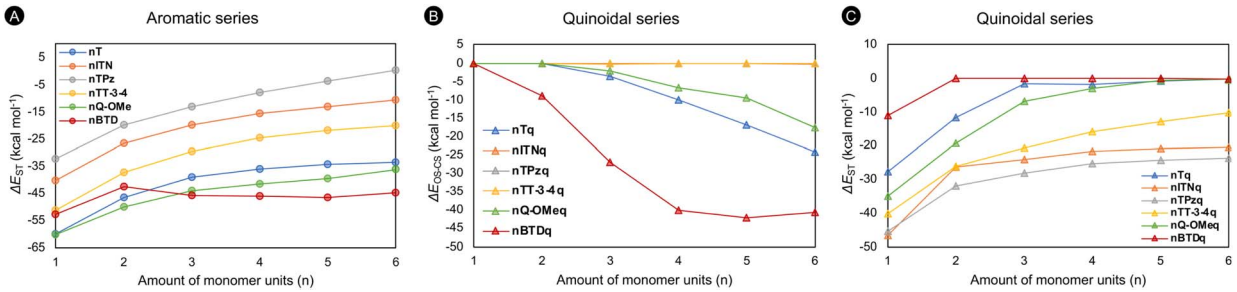

Fig. 2 (A) Variation of the adiabatic singlet–triplet gap (ΔE_{ST}) with chain length in the aromatic oligothiophenes. (B) Open-shell/closed-shell energy difference ($\Delta E_{OS\text{-}CS}$) in quinoidal oligothiophenes from the monomer to the hexamer. The curves of *n*ITNq and *n*TPzq are identical to that of *n*TT-3-4q, resulting in complete overlap and making them indistinguishable in the plot. (C) Adiabatic singlet–triplet gap (ΔE_{ST}) as a function of the number of repeat units (n) for the quinoidal oligomers.

indicative of a true diradical ground state. Fig. 3 clearly shows that the system progressively evolves into an open-shell singlet with enhanced diradical character as the number of units increases. A similar length-dependence of the diradical character for ***n*Tq** is observed using both unrestricted single-reference DFT methods (UPBE0 and UPBE0-DH) and multi-reference approaches (CASSCF(6,6) and CASSCF(12,12)) (Fig. S3). Based on this benchmark, the double-hybrid UPBE0-DH functional emerges as a suitable method offering a good compromise between accuracy and computational efficiency. In contrast, the aromatic series (***n*T**) shows no evidence of diradical character, fully consistent with their closed-shell ground structures. Similarly, y_0 remains 0 for the various annulated aromatic families, which can be attributed to the stabilizing effect of the aromatic thiophene rings (Table S11 and Fig. S4).

In the case of ***n*ITNq**, ***n*TPzq**, and ***n*TT-3-4q**, the open-shell calculations provide y_0 values of zero even for the longer oligomers, consistent with a preferred closed-shell singlet ground-state (Fig. 3). The presence of annulated aromatic rings in these quinoidal oligothiophenes effectively prevents the development of diradical character. In contrast, for the remaining quinoidal oligomers (***n*BTDq** and ***n*Q-OMeq**), y_0 increases with the number of repeat units, indicating an enhanced contribution of the diradical open-shell resonance structure as the chain lengthens. The impact of the benzoquinone-annulated ring in the ***n*BTDq** series is particularly pronounced, as it induces a rapid increase in diradical character, unlike the more gradual evolution of y_0 in the parent ***n*Tq** series. Notably, the dimer and trimer of ***n*BTDq** already exhibit y_0 values close to 1, and from the tetramer onward, the structures can be classified as pure diradicals. However, this gradual increase is observed for the ***n*Q-OMeq** series, consistent with the acquired trend for the energy gaps.

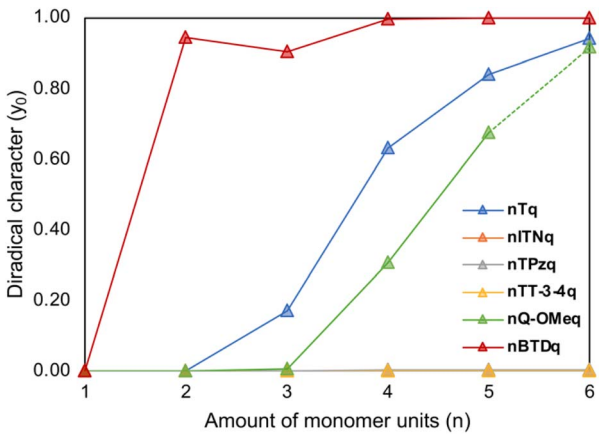

Fig. 3 Diradical character (y_0) as a function of the number of repeat units ($n = 1$ to 6) in quinoidal oligothiophenes calculated at the UPBE0-DH/6-31G(d) level of theory, with the exception for the results of **1-5Q-OMeq**, which were acquired with UPBE0/6-31G(d), and **6Q-OMeq**, which was obtained with UHF/6-31G(d).

Next, we examine the evolution of the HOMO–LUMO gap as a function of the oligomer length across the different series (Table S14). For the **1–6T** oligomers, a large HOMO–LUMO gap is expected,[145] which is indeed confirmed by our results evaluated at different levels of theory (Table S12 and Fig. S5–S6). In comparison, the ***n*Tq** derivatives exhibit significantly reduced band gaps, with **3–6Tq** displaying the overall smallest HOMO–LUMO gaps, consistent with their pronounced diradical character. Additionally, both series display a clear trend of decreasing HOMO–LUMO gap with increasing oligomer length, consistent with enhanced π-conjugation and electronic delocalization along the molecular backbone.[71,146] The narrowing of the HOMO–LUMO gap is observed in all aromatic and quinoidal series, except for the ***n*BTD** and ***n*BTDq** series, which maintains a relatively constant band gap despite elongation. The band gaps of the ***n*ITN**, ***n*TPz**, and ***n*TT-3-4** derivatives, featuring annulated aromatic rings, are significantly smaller than that of the parent ***n*T** compounds. Previous studies showed that benzene annulation onto the thiophene ring lowers the band gap by approximately 1 eV,[147,148] an effect well reproduced by our calculations. This band gap reduction has been attributed to the increased quinoid contribution to the electronic structure, which destabilizes the HOMO and stabilizes the LUMO.[148,149] Consistent with these findings, our results show that the HOMO–LUMO gap in the quinoidal series decreases further upon annulation with aromatic ring.

To assess the influence of steric hindrance on molecular geometry, we analyzed the planarity of optimized structures *via* average dihedral angles between adjacent monomers (see

Fig. S8 and S9). While most quinoidal compounds exhibit near-planar backbones, certain series show significant torsional distortion due to steric effects, which may influence their electronic structure. A comprehensive discussion of these findings is provided in the SI.

Local aromaticity and quinoidal/aromatic transformations (vertex 2)

Table 2 collects the values of the selected aromaticity indices of the central, inner, and outer five-membered rings of the parent oligothiophene series (***n*T** and ***n*Tq**). For HOMA, I_{ring}, and MCI, higher values indicate greater aromaticity, whereas for FLU, values closer to zero correspond to higher aromatic character. All aromaticity indices confirm that the thiophene rings in the ***n*T** series are highly aromatic. Although slight variations in aromaticity are observed among the inner, central, and outer rings depending on the specific index, the overall trend remains consistent, indicating that **1–6T** can be classified as locally aromatic. Nevertheless, when compared with isolated thiophene, a slight decrease in local aromaticity is observed as the oligomer length increases.

The trends in local aromaticity for the ***n*Tq** series are markedly different, with large variations in the structural and electronic indices as a function of the oligomer length. While the monomer and dimer are clearly nonaromatic with a well-defined quinoidal geometry, the transition to an open-shell singlet structure at $n = 3$ is accompanied by notable changes across all aromaticity indices. From the trimer onwards, the HOMA, FLU, MCI, and I_{ring} values gradually approach those of the aromatic ***n*T** series, indicating an increase in local aromatic character. The aromatization of the thiophene rings decreases from the central to the external rings (Table 2), suggesting that the quinoidal-to-aromatic transition initiates at the central ring(s) of the oligomer backbone. The aromatic stabilization, coupled to the double-bond weakening, results in a situation where, beyond a certain oligomer length, the closed-shell quinoidal structure becomes unstable and preferentially breaks a double bond to gain local aromaticity, thereby adopting a diradical ground state.[62–64]

This hypothesis is further corroborated by examining the influence of annulated rings on the local thiophene aromaticity, as illustrated by the MCI values of the central ring(s) of the oligomer backbone in Fig. 4A. In the aromatic series, most annulated derivatives exhibit a decrease in aromaticity compared to the parent ***n*T** series. The most significant decrease is observed in the local aromaticity of ***n*TT-3-4** and ***n*Q-OMe**. Among the three series where additional aromatic rings were annulated, the thiophene ring (***n*TT-3-4**), has the most significant impact, followed by pyrazine (***n*TPz**) and benzene (***n*ITN**),

Table 2 Structural and electronic aromaticity indices for the central, inner, and outer rings of the parent oligothiophene series (*n*T and *n*Tq) at the (U)CAM-B3LYP/cc-pVTZ level of theory. Only the **3–6Tq** oligomers exhibit an open-shell singlet ground state; all other oligothiophenes are closed-shell

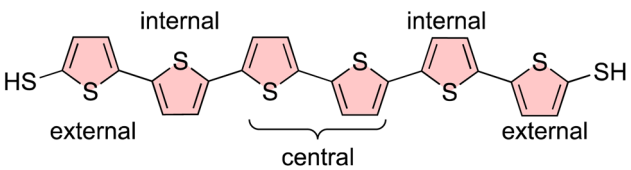

Type of ring(s)		HOMA	FLU	MCI	I_{ring}		HOMA	FLU	MCI	I_{ring}
Isolated ring	Thiophene	0.785	0.008	0.035	0.027	2,5-Dimethylene-2,5-dihydrothiophene	0.014	0.039	0.004	0.006
Central ring	**1T**	0.780	0.006	0.030	0.025	**1Tq**	0.090	0.038	0.004	0.007
Central rings	**2T**	0.790	0.005	0.028	0.023	**2Tq**	0.201	0.034	0.005	0.007
Central ring	**3T**	0.798	0.005	0.025	0.022	**3Tq**	0.767	0.007	0.011	0.012
External rings		0.790	0.005	0.027	0.023		0.612	0.014	0.008	0.010
Central ring(s)	**4T**	0.797	0.005	0.025	0.022	**4Tq**	0.824	0.003	0.018	0.017
External rings		0.790	0.005	0.027	0.023		0.739	0.008	0.010	0.011
Central ring	**5T**	0.795	0.005	0.024	0.021	**5Tq**	0.807	0.004	0.022	0.020
Internal rings		0.797	0.005	0.025	0.021		0.817	0.003	0.020	0.018
External rings		0.789	0.005	0.027	0.023		0.758	0.007	0.011	0.012
Central rings	**6T**	0.796	0.005	0.024	0.021	**6Tq**	0.800	0.004	0.023	0.021
Internal rings		0.796	0.005	0.025	0.021		0.812	0.004	0.021	0.019
External rings		0.790	0.005	0.027	0.023		0.765	0.006	0.011	0.012

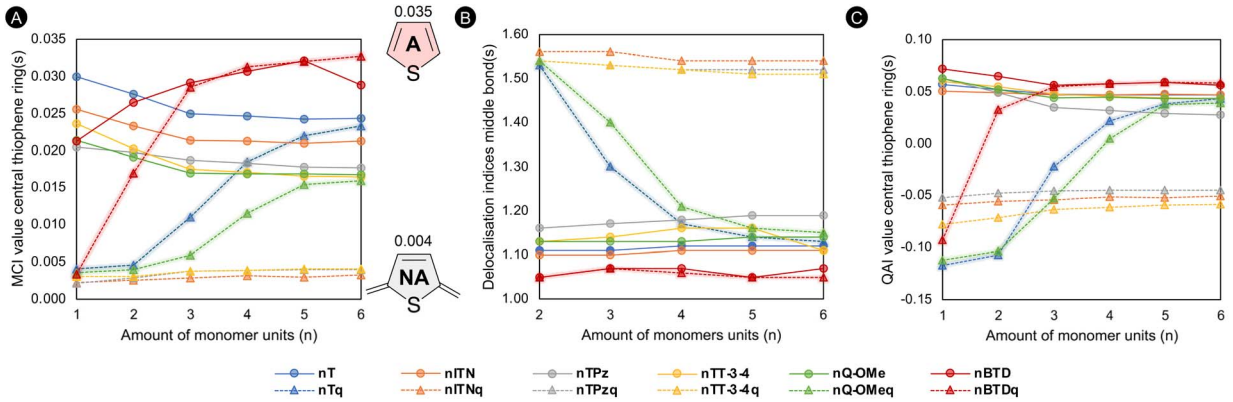

Fig. 4 (A) Evolution of the MCI index of the central thiophene ring(s) with the chain length of the investigated oligomers. (B) The delocalization index of the middle bond(s) as a function of number of the repeat units. (C) The quinoidization/aromatization index (QAI) of the central rings quantified based on selected C–C bond distances. All indices computed at the (U)CAM-B3LYP/cc-pVTZ level of theory. Thiophene and 2,5-dimethylene-2,5-dihydrothiophene are included as reference structures.

respectively. Among all aromatic series, only ***n*BTD** oligomers display a sharp increase in local aromaticity with increasing chain length, surpassing even the ***n*T** series from the trimer onwards.

Regarding the quinoidal families, the central thiophene rings of ***n*ITNq**, ***n*TPzq**, and ***n*TT-3-4q** exhibit minimal changes in local aromaticity, consistent with their closed-shell character and the preservation of the quinoidal structure. In contrast, systems adopting an open-shell singlet configuration exhibit a pronounced increase in the local aromaticity of the thiophene subunits. This effect is particularly striking in the ***n*BTDq** series, where aromaticity rises sharply from the dimer, approaching the MCI values computed for the corresponding aromatic ***n*BTD** series. For large n values, several aromatic and quinoidal series converge toward similar MCI values in the central thiophene ring(s), as observed in pairs such as ***n*T**/***n*Tq**, and ***n*Q-OMe**/***n*Q-OMeq**.

Building on the proposed relationship between the MCI and y_0, the variation of the MCI index for the central thiophene ring(s) as a function of the diradical character was analyzed (Fig. 5). This analysis yielded a determination coefficient of $R^2 = 0.89$, thereby substantiating a clear relationship between diradical character and local aromaticity, two vertices of the triangle in Fig. 1.

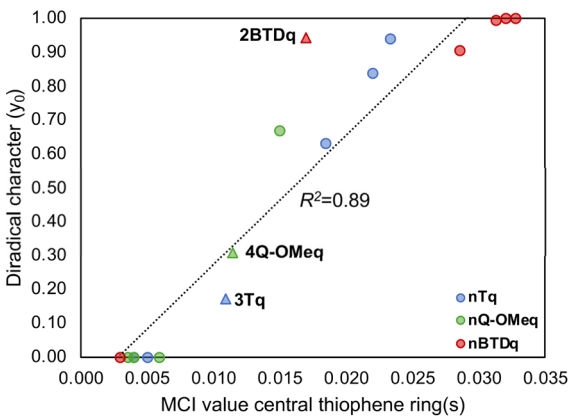

Fig. 5 Correlation plot between the MCI values of the central thiophene ring(s) and the diradical character (y_0) for the quinoidal oligothiophenes *n*Tq, *n*Q-OMeq, and *n*BTDq. The first open-shell singlet structure within each series is marked with a triangle.

In light of these observations, it is worthwhile to examine how the annulated rings influence each other's local aromaticity to provide deeper insight into the observed trends. To assess the degree of aromaticity in the annulated rings, we employ the normalized $MCI^{1/n}$ index, which enables a meaningful comparison across rings of different sizes.[150] Fig. 6 illustrates the variation in $MCI^{1/n}$ for individual rings across selected oligomers using a color scale based on the aromaticity of selected reference compounds. Applying this approach to the rings of ***n*ITN** reveals that the backbone thiophene rings are less aromatic than the annulated benzene rings. When compared to the isolated monocyclic units, it becomes clear that both the thiophene ring and the annulated six-membered ring exhibit reduced local aromaticity upon incorporation into the oligomer backbone. This observation suggests that benzannulation reduces the aromatic stabilization of the individual subunits, while enhancing the delocalization along the linking single bonds (Fig. 4B). This effect favors the quinoidal resonance contribution.[71,146,151] In contrast, annulation with a cross-conjugated ring, as in the ***n*BTD** series, enhances the local aromaticity of the backbone thiophene rings starting from the trimer, further stabilizing the aromatic resonance structure compared to the unsubstituted ***n*T** series and decreasing the delocalization index of the linking C–C bonds (Fig. 4B).

For the monomers of quinoidal structures, the effect of additional fused rings on the thiophene is less pronounced (Fig. 6). As expected, the backbone thiophene rings are all nonaromatic, whereas the annulated benzene, pyrazine, and thiophene rings are highly aromatic, surpassing their local aromaticity in the corresponding aromatic series. An inverse relationship is observed, where an increase in the aromaticity of the annulated ring corresponds to a decrease in the local aromaticity of the adjacent thiophene. $MCI^{1/n}$ values further indicate that the fusion of cyclopentane and benzoquinone

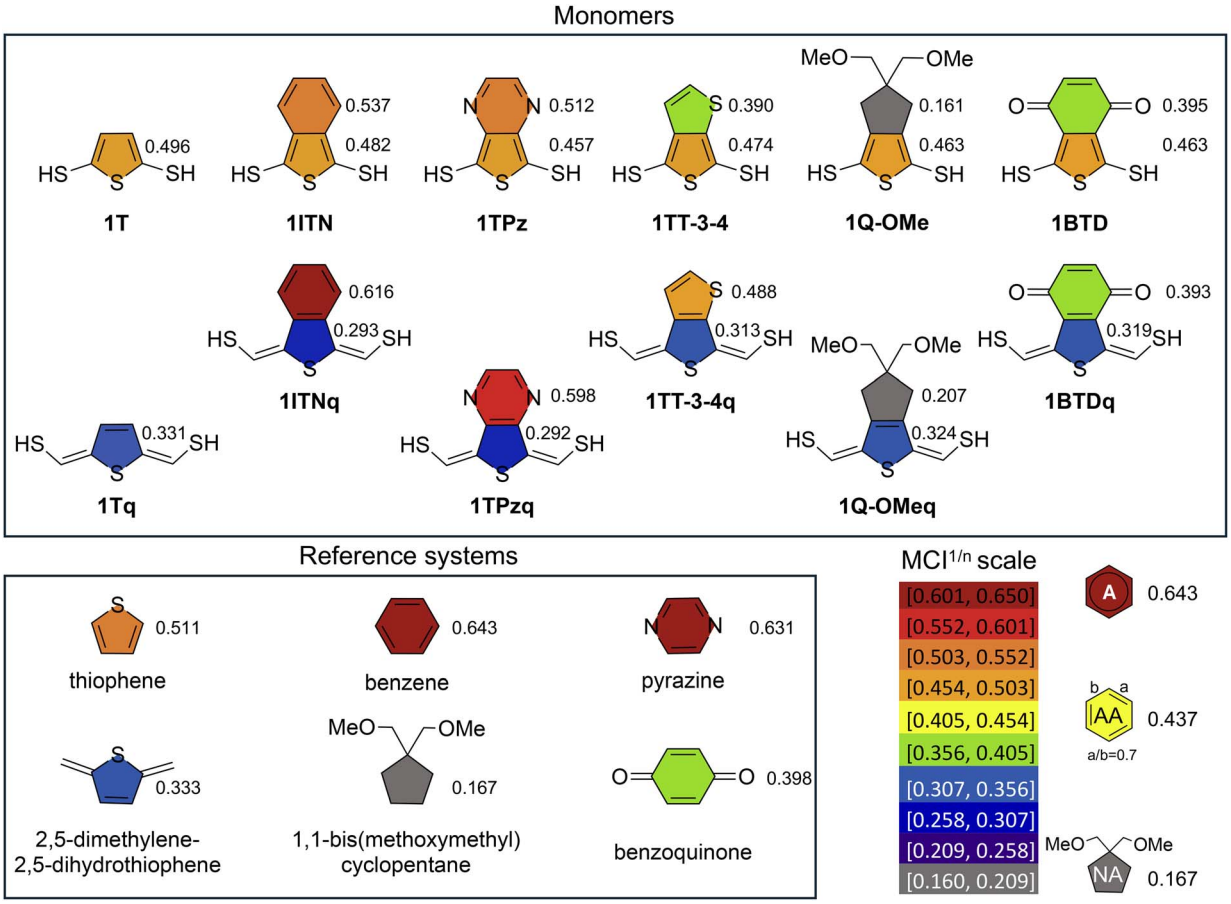

Fig. 6 Local aromaticity of the monomers and selected reference compounds represented by the normalized $MCI^{1/n}$ values, computed at the CAM-B3LYP/cc-pVTZ level of theory.

rings has a minimal influence on the thiophene aromaticity in the monomers. The quinoidal-to-aromatic transition observed in several quinoidal oligothiophenes (***n*Tq**, ***n*BTDq**, and ***n*Q-OMeq**) can be sclearly visualized by color-coding the individual rings according to the normalized MCI values, as illustrated in Fig. 7. Regarding the ***n*Tq** series, a large difference in the local aromaticity of the central thiophene ring is evident when comparing the closed-shell dimer (**2Tq**) with the open-shell singlet trimer (**3Tq**). Oligomer length also plays an important role in modulating the aromatization of the individual rings, as evidenced by **3Tq** and **5Tq** structures. In both cases, the central rings display significantly higher aromaticity than the terminal thiophene units, emphasizing the localized aromatic character of the quinoidal-to-aromatic transition. Similar trends are

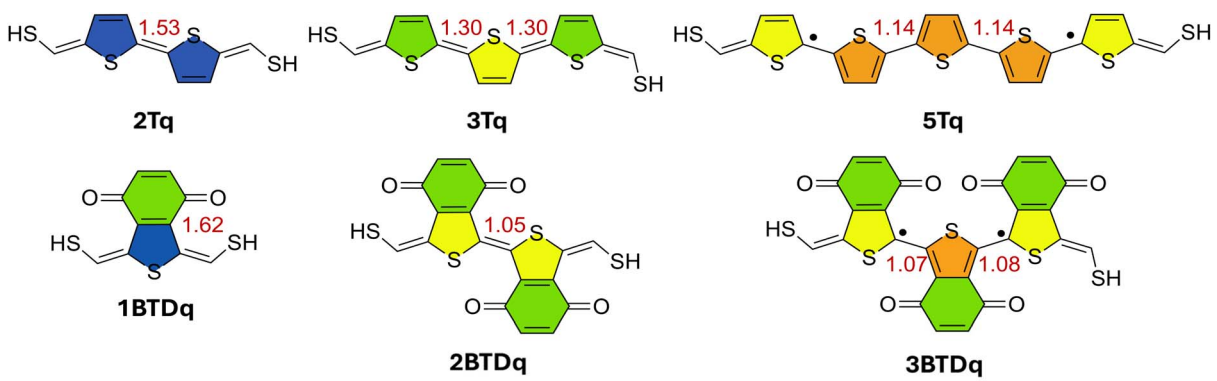

Fig. 7 Gradual change in local aromaticity of the thiophene rings during the transition from closed-shell quinoidal to open-shell aromatic structures. Each ring is color-coded according to its $MCI^{1/n}$ values. The color scale is provided in Fig. 6. The delocalization index of selected C–C bonds is shown in red.

observed for the ***n*BTDq** (Fig. 7) and ***n*Q-OMeq** oligomers (Fig. S13). In both cases, the transition from closed- to open-shell configurations, occurring at $n = 2$ for ***n*BTDq** and $n = 3$ for ***n*Q-OMeq**, leads to a pronounced increase in the local aromaticity of the backbone rings, starting from the central units. The observed trends in local aromaticity can only be rationalized by the formation of unpaired electrons resulting from the double bond cleavage. This analysis reveals, for the first time, that MCI serves as a direct and quantitative indicator of diradical character in quinoid-type systems. Consistent with several benchmark studies, MCI emerges as one of the most reliable descriptors, outperforming traditional aromaticity indices such as HOMA and NICS, which are respectively sensitive to reference parameters and influenced by σ- and π-contributions.[152,153] Further insight into the quinoidal-to-aromatic transition is provided by the delocalization indices (DI) of the C–C bonds linking the central rings (Fig. 4B), which reveal a strong correlation between changes in electronic structure and deviations from the quinoidal geometry (Fig. S15–S25). A DI larger than 1.5, observed for ***n*ITNq**, ***n*TPzq**, and ***n*TT-3-4q**, as well as **1–2Tq** and **1-2Q-OMeq**, indicates significant double-bond character, showing that the quinoidal structure is largely preserved in these oligomers. Conversely, a low DI (∼1.15) indicates single-bond character. In ***n*Tq** and ***n*Q-OMeq** series, a gradual decrease in DI is observed with increasing chain length, consistent with trends in MCI and y_0 values. This decline signals the transformation from quinoidal to aromatic diradicaloid species as the number of monomers increases. In contrast, the DI values for ***n*BTDq** do not exhibit such gradual transition, instead converging to those of the aromatic counterpart (***n*BTD**) already at the dimer. Likely, the steric hindrance between the repeat units and the large torsion angles (Fig. S9) prevent the double-bond formation.

Finally, the geometrical quinoidization/aromatization index (QAI), derived from the differences in C–C bond distances within the thiophene rings,[62,63] confirms the quinoidal-to-aromatic transitions (Table S41). Consistent with the MCI and DI trends, Fig. 4C shows that the QAI parameter changes drastically on increasing the size of the oligomer in ***n*Tq**, ***n*Q-OMeq**, and ***n*BTDq**. All open-shell systems exhibit positive QAI values, except for the **3Tq** and **3Q-OMeq** trimers. Although their central ring shows a notably lower QAI value than the outer rings, the overall structure retains its quinoidal character, as confirmed by the DI values. The QAI also supports the observation that the aromatization of the conjugated backbone in **4–6Tq** and **4-6Q-OMeq** is restricted to the central and internal thiophene rings, while the terminal rings maintain a quinoidal structure. The ***n*BTDq** oligomers are unique since all backbone rings exhibit positive QAI values from the dimer onwards. These values closely match those of the corresponding ***n*BTD** structures, indicating a similar backbone geometry modified by the presence of two unpaired electrons. The remaining closed-shell quinoidal oligomers exhibit negative QAI values (Table S41) consistent with a quinoidal ground state. In contrast, all aromatic families show positive QAI values, indicating that the backbone rings adopt a geometry resembling that of the isolated thiophene molecule.

In summary, the QAI descriptor provides an efficient and intuitive tool for detecting the closed-shell quinoidal to aromatic diradical transformation in quinoidal oligothiophenes, as well as identifying the specific oligomer length at which this transition occurs. Since it requires only a single geometry optimization, QAI is particularly well-suited for fast screening across large oligomer databases. Moreover, when combined with MCI and DIs, QAI offers a comprehensive view of the structural and electronic evolution as the chain length increases along the oligomer series.

Single-molecule conductance (vertex 3)

We now explore how variations in oligomer length, diradical character, and aromaticity affect the conductance of the oligothiophenes at the molecular scale, shedding light on their potential as molecular wires.

Fig. 8 shows the transmission spectra of the parent aromatic (***n*T**) and quinoidal (***n*Tq**) oligothiophene series. For the ***n*T** series, the transmission around the Fermi level decreases progressively with increasing number of monomer units. This trend is also evident in the conductance *versus* molecular length plot in Fig. 8C, which reveals ohmic behavior for the aromatic closed-shell structures. As the chain lengthens, the rate of conductance decay gradually decreases. The result for the **4T** oligomer aligns well with the findings reported by Ohto *et al.*,[54] further validating the computational approach employed in this study (Fig. S26). The conductance data of ***n*T** are consistent with a tunneling transport mechanism in the short-chain regime, in agreement with previous works.[47–49,59]

However, the quinoidal ***n*Tq** series exhibits distinct behavior for the dimer (**2Tq**) and trimer (**3Tq**). Their transmission spectra reveal an increase in conductance with the addition of monomer units, an indication of anti-ohmic behavior (Fig. 8C). From **4Tq** onward, ohmic behavior reemerges, although the transmission spectra remain notably shifted.

This transition can be plausibly attributed to the interplay between two opposing effects. On the one hand, the growing tendency toward diradical character enhances conductance.[21–24,49] This effect emerges at $n = 2$ and plateaus at higher n values within the open-shell regime ($n = 3$–6). On the other hand, this increase is counterbalanced by a length-dependent attenuation of conductance, which inevitably leads to near-zero values as the molecular chain extends. Molecules with lengths approaching 20 Å typically exhibit negligible conductance,[28] a threshold exceeded by the sulfur-to-sulfur linker distance in the pentamer and hexamer structures of our series. These opposing factors may result in a conductance maximum, as observed here for $n = 3$, consistent with prior experimental observations in cationic oligophenylene-bridged bis(triarylamines).[26] A relatively high conductance is also observed for $n = 4$, which could be attributed to the increasing diradical character not yet being fully offset by the length-dependent attenuation. Although the transmission spectra and conductance values differ slightly between α and β spins in open-shell structures, the observed trends are identical

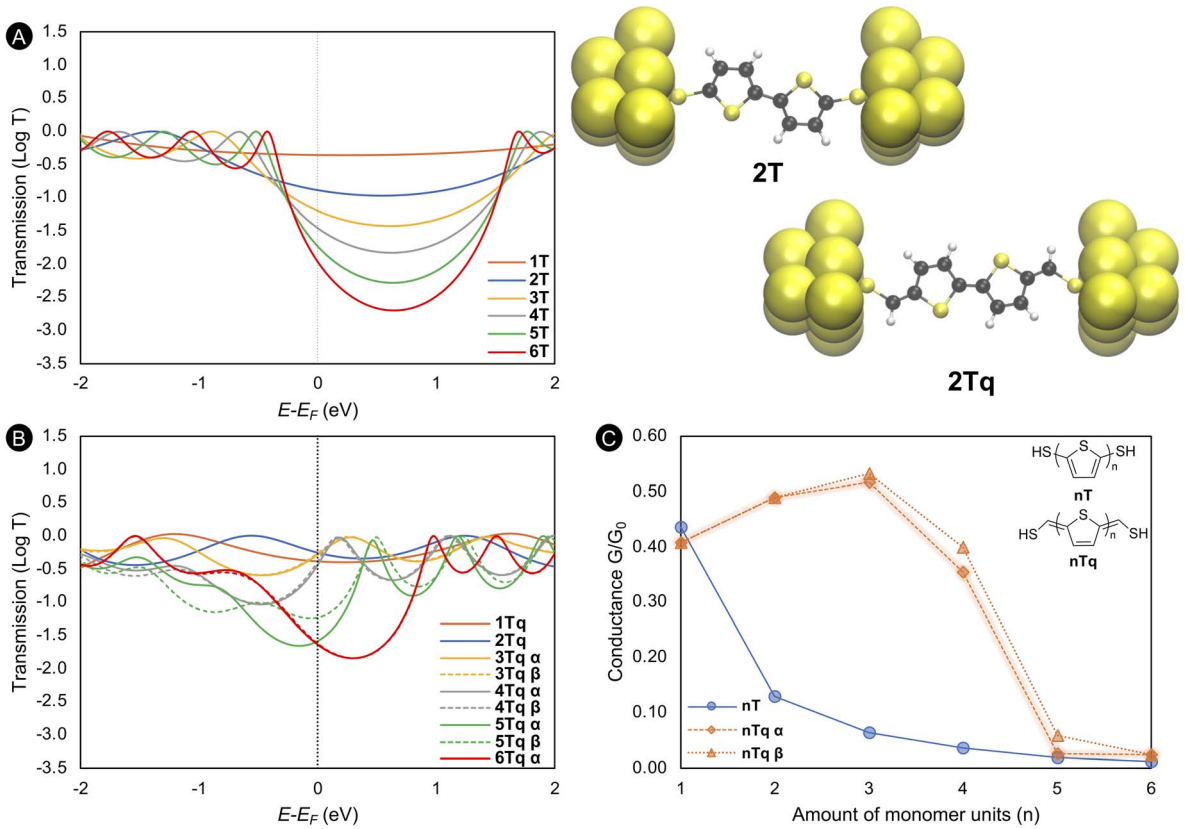

Fig. 8 Transmission spectra of the parent aromatic (*n*T) oligothiophenes (A) and the quinoidal (*n*Tq) series (B). The molecular junction geometries for the corresponding dimers (2T and 2Tq) are also shown. (C) Theoretical conductance values (G/G_0) plotted as a function of the number of monomer units.

(Fig. 8C). Therefore, only α-spin results are discussed henceforth.

Comparing the conductance of the aromatic and quinoidal parent compounds, only **1Tq** exhibits a slightly lower conductance than its aromatic counterpart. In contrast, the pentamers and hexamers of both series display similarly low conductance values, as expected based on the preceding discussion. To further ensure the robustness of this anchoring choice, additional calculations were performed for the parent aromatic and quinoidal oligothiophenes (***n*T** and ***n*Tq**) using pyridine and NH_2 anchoring groups. The results demonstrate that the main transmission features and overall length-dependent conductance trends remain consistent across different anchoring groups (Fig. S27 and S28).

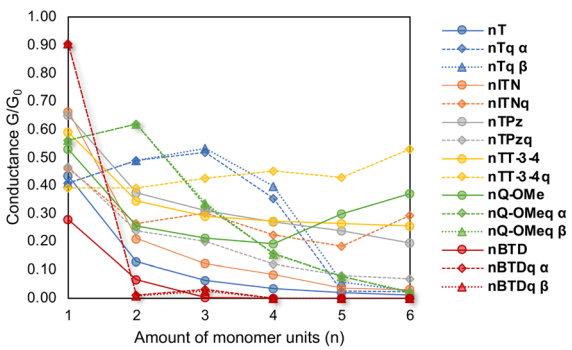

Fig. 9 Evolution of the conductance as a function of the oligomer length in aromatic and quinoidal compounds.

The conductance of the functionalized oligothiophenes are shown in Fig. 9. The incorporation of annulated rings has a noticeable effect on the transmission spectra and conductance compared to the parent series (Fig. S29 and S30). In oligothiophenes where annulated rings reduce the aromaticity of the thiophene backbone, the characteristic parabolic shape of the transmission spectra between the HOMO and LUMO is preserved, albeit shifted along the energy axis. This parabolic profile is indicative of a constructive quantum interference (CQI).[35] In contrast, the fusion of cross-conjugated rings significantly alters the shape of the transmission spectra, giving rise to a shifted destructive quantum interference (SDQI).[38] This SDQI lead to reduced conductance values at the Fermi level, particularly in **4–6BTD** systems.

Aromatic oligothiophenes exhibit ohmic behavior (Fig. 9). An overall increase in conductance is observed compared to the parent ***n*T** series, except for the ***n*BTD** series due to the impact of cross-conjugation. In general, compounds with annulated rings that reduce the aromaticity of the thiophene backbone (*e.g.* ***n*ITN**, ***n*TT-3-4**, and ***n*TPz**) display higher conductance than the parent oligomers. Notably, the results for **5Q-OMe** and **6Q-OMe**

deviate from the expected trend, exhibiting unexpectedly high conductance values. The origin of this deviation remains unclear.

Turning to the conductance near the Fermi level for quinoidal oligothiophenes (Fig. 9), conductance is generally higher than in the aromatic series, consistent with their smaller HOMO–LUMO gaps. Elevated conductance values are associated with annulated rings that strongly reduce the aromaticity of the thiophene units. The evolution of conductance in ***n*Q-OMeq** is particularly noteworthy, showing a shift from anti-ohmic to ohmic behavior as the system transitions toward an open-shell diradical configuration with increased oligomer length. As in the ***n*Tq** series, we suspect that the observed trend arises from the interplay between emerging diradical character and the opposing effect of increasing molecular length on electron transport. The ***n*BTDq** series was anticipated to follow a similar trend, but the early onset of diradical character (already at the dimer) prevented the transition from anti-ohmic to ohmic behavior from taking place. These findings suggest that when the diradical character becomes excessively large ($y_0 \approx 1$), conductance approaches zero regardless of the oligomer length.

Two additional quinoidal series, ***n*ITNq** and ***n*TPzq**, exhibit ohmic behaviour. Among them, the incorporation of a benzene ring results in slightly higher conductance compared to the annulated pyrazine. Finally, the ***n*TT-3-4q** series exhibits a relatively constant conductance across increasing oligomer lengths and does not clearly exhibit either ohmic or anti-ohmic behaviour.

In conclusion, charge transport calculations reveal that, except for $n = 1$, the quinoidal ***n*Tq** compounds exhibit higher conductance than the aromatic ***n*T** counterparts. This trend correlates with the enhanced diradical character and narrower HOMO–LUMO gap in the quinoidal oligothiophenes and may underlie the anti-ohmic behaviour observed from the monomer to the trimer in this series. Upon annulation, conductance increases in the aromatic oligothiophenes, particularly for fused rings that induce a significant reduction in the aromaticity of the thiophene units. In contrast, cross-conjugated fused rings enhance the aromaticity of the thiophene units and consequently reduce conductance. In the quinoidal systems, annulated derivatives generally maintain higher conductance than their aromatic analogues, mirroring the behaviour of the parent series. Notably, the ***n*Q-OMeq** series, featuring a saturated five-membered ring fused to the thiophene backbone, exhibits an initial anti-ohmic trend, similar to that of the ***n*Tq** parent series.

The net current through the oligomer series can be visualized using the local transmission plots (LTPs) shown in Fig. 10 for the parent ***n*T** and ***n*Tq** compounds. The predominant transmission pathways are indicated by arrows, with arrow width proportional to the atom–atom transmission values.[133] These plots can be interpreted with the help of the DIs (Fig. S15–S25) and the linear aromaticity pathway (Fig. S31–S40), also referred to as the "most aromatic pathway", which is likewise depicted in Fig. 10 for the parent series. The DI-based pathway is determined by connecting the two anchoring thiol groups through the bonds with the highest DI, while the LAP is identified by selecting the most conjugated pathway, characterized by the highest AV_{min} values.[35,37,38,41,44]

In the context of the "triangle", the key question is whether the preferred transmission pathway aligns with the most aromatic one, linking conductance and aromaticity, unlike the previous section, which considered overall conductance. A positive outcome would support using aromaticity descriptors to predict dominant transmission pathways, potentially reducing the need for entire junction calculations.

As shown in Fig. 10, the dominant transmission pathway identified by the LTPs exhibits a higher net current through the carbon–carbon bonds within the thiophene subunits. Nonetheless, a small fraction of the current still flows through the carbon–sulfur–carbon (CSC) bonds, especially in the ***n*T** oligomers and the **1–2Tq** structures. A marked change is observed in the **3–6Tq** compounds, where the current bypasses the CSC bonds with the threshold set to 20% of the maximum atom–atom transmission. This shift closely parallels the transition from closed-shell to open-shell singlet configurations. Notably, there is excellent agreement between the DI values, LAPs, and LTPs across all ***n*T** and ***n*Tq** oligomers. Furthermore, no differences in the preferential pathways were observed between the α-

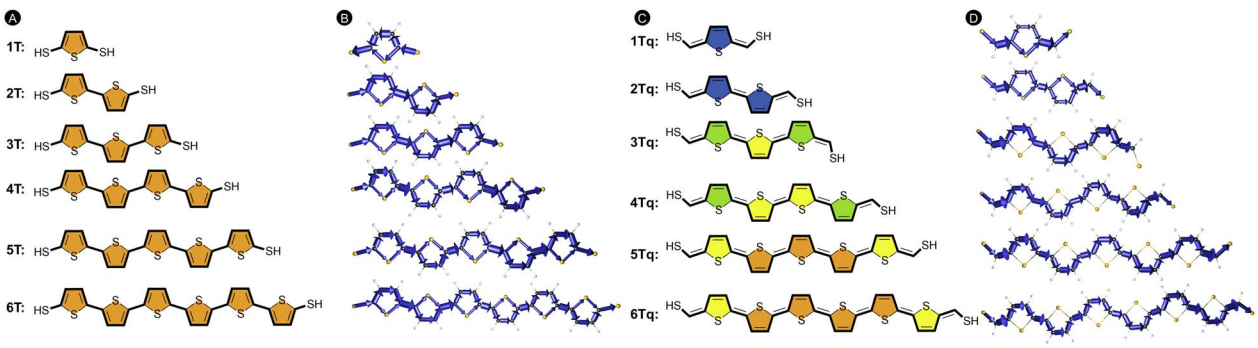

Fig. 10 Linear aromaticity pathways and local transmission plots for the parent oligothiophenes. (A) and (C) The most aromatic pathway depicted as black bonds according to the electronic AV_{min} index. The individual rings are colored according to the normalized $MCI^{1/n}$ values using the scale displayed in Fig. 6. (B) and (D) Local transmission plots with the blue arrows indicating the net current flowing from left to right with the threshold set to 20% of the maximum atom–atom transmission.

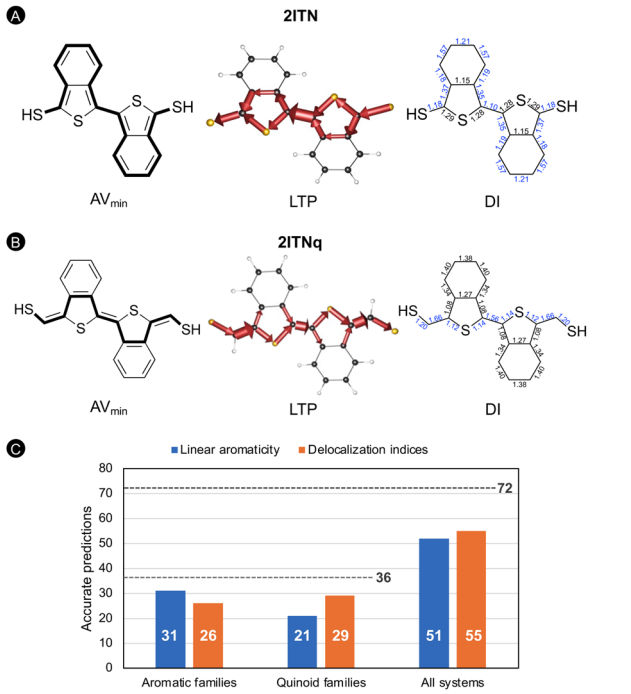

Fig. 11 Local transmission plots alongside the predicted most conjugated pathways based on the DIs and AV_{min} values for **2ITN** (A) and **2ITNq** (B). (C) Number of correct pathway predictions by the linear aromaticity calculations and delocalization indices for aromatic and quinoidal oligothiophenes as well as the total number of correct predictions across all oligomers.

and β-spin channels in the open-shell oligomers (Fig. S41 and S43).

The parent oligomers exhibit a limited number of available pathways for electron transport. Incorporating annulated rings significantly increases the number of possible pathways, which can complicate accurate predictions. This effect is already evident in the ***n*ITN** family, as illustrated in Fig. 11A for the dimer (Fig. S31). Despite the structural complexity, the LTPs remain confined to the backbone thiophene, a trend that continues for larger oligomers as well. These LTPs resemble the transmission pathways observed in the ***n*T** compounds, suggesting that the addition of a benzene ring has minimal influence on the preferred conduction pathway in the aromatic oligothiophenes. In contrast, the main conjugation pathway predicted from the DIs and AV_{min} incorporates the annulated benzene in all the cases, except for the monomer (Fig. 11A).

The LTPs of the ***n*ITNq** quinoidal structures indicate that electrons preferentially follow the shortest path between the electrodes, resulting in the CSC bonds contributing most significantly to conduction (Fig. 10D and S32). The incorporation of annulated benzene rings alters the preferred transmission pathways compared to the parent ***n*Tq** oligomers. The DIs accurately predict this pathway for all six structures. However, the LAPs only align with this outcome for the monomer. Evidently, the DI and LAP methods do not always yield consistent results.

A comprehensive analysis of the local transmission plots for all remaining oligothiophenes (Fig. S31–S43) was conducted to assess the predictive accuracy of the DI and LAP approaches (Fig. 11C). In the aromatic families (36 oligomers), the LAP successfully predicted 31 pathways (86%), while the DIs predicted 26 (72%). For the quinoidal series (36 oligomers), the DIs performed better, correctly predicting 29 pathways (81%) compared to 21 (58%) for the LAP. These findings indicate that predictive accuracy depends on the structural family, and that the DIs and AV_{min} approaches do not always converge on the same most conjugated pathway. Consequently, we recommend using both techniques in parallel to enhance the reliability of identifying the preferred transmission pathways. Overall, AV_{min} correctly predicted 72% of all transmission pathways, while the DI-based approach predicted 76%, corresponding to 51 and 56 out of 72 oligomers, respectively (Fig. 11C). A detailed analysis of the few discrepancies between the AV_{min}-derived conjugated pathways and the LTPs indicates that these deviations primarily stem from methodological and computational limitations rather than from intrinsic inconsistencies between aromaticity and charge-transport descriptors (see SI).

Disentangling the triangle

This study fundamentally explores the interrelationships among diradical character, aromaticity, and conductance, as pictorially represented in the triangle in Fig. 1. Initial connections between these vertices emerged during the investigation of individual components. In this section, we aim to provide a more comprehensive overview of their interdependence. Based on our explorations, the aromaticity vertex is now divided into two components: one addressing the local aromaticity of the backbone thiophene rings and their annulated analogues, and the other focused on the concept of linear aromaticity pathways. This distinction naturally extends to the conductance vertex, which is likewise divided into overall conductance and local transmission pathway.

It is important to reiterate that, unlike conductance, which can be probed both experimentally and theoretically, diradical character and aromaticity are theoretical concepts not directly accessible through experiments.[14–20] Multiple theoretical indices have been developed to quantify these properties, and both have been widely correlated with experimentally measurable quantities. In the case of aromaticity, extensive literature has established numerous criteria—energetic, geometrical, electronic, magnetic, and reactivity-based—demonstrating its multifaceted nature.[112–120] Similarly, recent advances in the study of diradical character have connected it to reactivity and magnetic properties,[69] yielding several theoretical criteria. In this work, we adopt Yamaguchi's method as a measure of diradical character.[99] Given their theoretical nature, both vertices must be described on a solid and common ground: the electronic structure of the ground state. Their fundamental "ancestor" provides critical insights into the singlet or triplet nature of the system and whether it adopts an open- or closed-shell singlet configuration. As illustrated in Fig. 12, the two lower vertices of the triangle—aromaticity and diradical

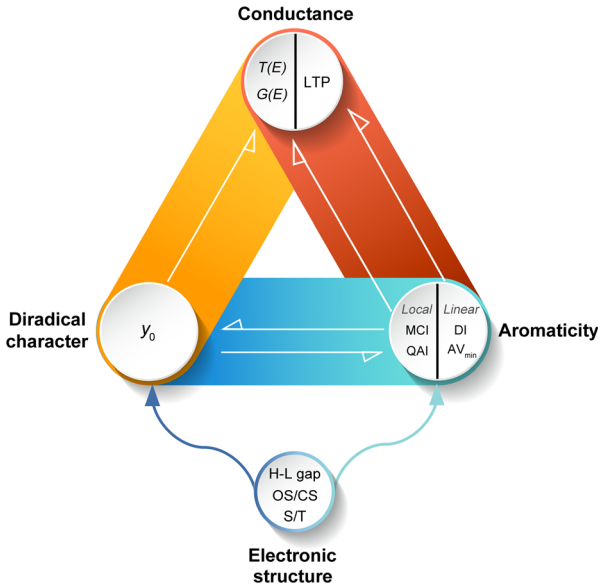

Fig. 12 The extended conductance-aromaticity-diradical character triangle.

character—are therefore conceptually linked to a fourth, supplementary vertex: the ground-state electronic structure, which supplies the essential data for their characterization.

Regarding the aromaticity vertex, we reiterate that only the aromaticity of individual backbone rings was considered, not the global aromaticity of the entire molecule. It is also worth noting that multiple descriptors were employed to characterize the local aromaticity. These descriptors demonstrated internally consistent behaviour across all series. Throughout our study, connections between the local aromaticity and diradical character have been established by examining the electronic structure across different oligothiophenes.

The aromatic oligomers, which uniformly adopt a closed-shell singlet ground state, exhibit strongly aromatic backbone rings according to all aromaticity indices, and show no diradical character. In contrast, several quinoidal families undergo a closed-shell to open-shell transition, leading to a discontinuity in the aromaticity trend of the backbone rings. Notably, the aromaticity of the central thiophene rings increases, ultimately approaching the values observed in their aromatic counterparts. This transition is consistently accompanied by a rise in diradical character. The strong, bidirectional correlation between the MCI values of the central rings and the diradical character is particularly striking. These two properties evolve in tandem—one does not change without the other—justifying the use of a double-headed arrow to represent their interdependence. This double arrow, however, will not be used when discussing connections to conductance, since the aim there is to relate a theoretically derived concept to an experimentally accessible property.

The sides of the triangle connecting conductance-diradical character and conductance-aromaticity reveal interrelated behaviours, particularly in light of the established correlation between aromaticity and diradical character. The relationship between conductance and diradical character involves a delicate interplay of two opposing effects: increasing diradical character generally enhances conductance, but this is counteracted by a length-dependent attenuation that causes conductance to approach zero in sufficiently long systems (typically beyond ~20 Å).[28] Moreover, when the diradical character becomes excessively high ($y_0 \approx 1$), conductance diminishes regardless of oligomer size.

Focusing on the conductance-aromaticity vertex, a clear pattern emerges in the aromatic series: annulated rings that most strongly reduce the aromaticity of the backbone thiophene units result in higher conductance compared to the parent compounds. Interestingly, nonaromatic fused rings produce a similar effect. In contrast, the incorporation of cross-conjugated rings tends to increase the aromaticity of the thiophene subunits and consequently leads to lower conductance.

Up to this point, our focus has been on the overall conductance and the backbone aromaticity components of their respective vertices. Shifting attention to the local aspects, namely, the local transmission pathways and the most conjugated pathways, a clear relationship emerges. The local transmission plots show strong correspondence with pathway predictions based on delocalization indices and the AV_{min} index. Together, these aromaticity-based descriptors successfully identify the preferred transmission routes in approximately 70% of the investigated oligothiophenes, demonstrating their utility as predictive tools for local charge transport behaviour.

Conclusions

Exploring the fundamental relationships of the diradical character-aromaticity–conductance triangle was the leitmotiv of this study. A diverse set of oligothiophenes, capable of adopting both aromatic and quinoidal structures, was selected as the molecular testbed. The original triangle (Fig. 1) revealed multiple connections between the three vertices. Through our investigation, this framework was refined by introducing the electronic ground-state structure as a new vertex, subdividing the aromaticity and conductance vertices into global and local components, and denoting, *via* a double-headed arrow, the intrinsic relationship between the diradical character and aromaticity vertices (Fig. 12). This extended triangle offers a more nuanced view of the shared origin of the theoretical descriptors and their relationship to an experimentally accessible property, molecular conductance. While the basic structure of the original triangle is preserved, its content is now significantly deepened and rendered more insightful.

Author contributions

M. A. conceptualized the project. L. V. N., I. C. R., S. M. Q., and J. E. performed all quantum chemical calculations. F. D. P., P. G., and M. A. supervised the project. The first draft of the manuscript was written by L. V. N., P. G., and M. A. All authors were involved in future editing and reviewing process. All authors

have read and agreed to the published version of the manuscript.

Conflicts of interest

There are no conflicts to declare.

Data availability

The optimized Cartesian coordinates (XYZ files) of the molecular structures discussed in this work are available from the corresponding authors upon request. All other data supporting the findings of this study are available in the published article and/or the Supporting Information (SI). Supplementary information: oligothiophene nomenclature; adiabatic energy differences; spin-flip vertical energy gaps; diradical character; band gaps; geometrical aspects; aromaticity indices and theoretical background; transmission spectra and conductance; local transmission plots; and linear aromaticity. See DOI: https://doi.org/10.1039/d5sc05918f.

Acknowledgements

L. V. N., I. C. R., S. M. Q., F. D. P., and M. A. thanks the VUB for the Strategic Research Program awarded to the ALGC research group. J. E. acknowledges the Fonds Wetenschappelijk Onderzoek-Vlaanderen (FWO) for the support under the form of a predoctoral fellowship (1148524N). L. V. N. acknowledges the Fonds Wetenschappelijk Onderzoek for the support under the form of a predoctoral fellowship (1140226N). SMQ thanks Wetenschappelijk Onderzoek-Vlaanderen (FWO) for the support under the form of a junior postdoctoral fellowship (1267725N). I. C. R. acknowledges co-funding from the European Union's Horizon 2020 research and innovation Maria Skłodowska-Curie Actions (grant agreement number 945380) and DIPC. The computational resources and services used in this work were provided by the VSC (Flemish Supercomputer Center), funded by the Research Foundation – Flanders (FWO) and the Flemish Government.

Notes and references

† For oligothiophenes with multiple LAPs yielding the same AV_{min} value, the pathway with the highest AV1245 among them was selected.

1 A. Aviram and M. A. Ratner, Molecular rectifiers, *Chem. Phys. Lett.*, 1974, **29**, 277–283.
2 T. A. Su, M. Neupane, M. L. Steigerwald, L. Venkataraman and C. Nuckolls, Chemical principles of single-molecule electronics, *Nat. Rev. Mat.*, 2016, **1**, 1–15.
3 D. Xiang, X. Wang, C. Jia, T. Lee and X. Guo, Molecular-scale electronics: from concept to function, *Chem. Rev.*, 2016, **116**, 4318–4440.
4 N. Xin, J. Guan, C. Zhou, X. Chen, C. Gu, Y. Li, M. A. Ratner, A. Nitzan, J. F. Stoddart and X. Guo, Concepts in the design and engineering of single-molecule electronic devices, *Nat. Rev. Phys.*, 2019, **1**, 211–230.
5 J. Liu, X. Huang, F. Wang and W. Hong, Quantum interference effects in charge transport through single-molecule junctions: detection, manipulation, and application, *Acc. Chem. Res.*, 2018, **52**, 151–160.
6 K. Wan and B. Xu, in *Molecular-Scale Electronics: Current Status and Perspectives*, X. Guo, Springer International Publishing, Cham, 2019, pp. 1–43.
7 L. Sun, Y. A. Diaz-Fernandez, T. A. Gschneidtner, F. Westerlund, S. Lara-Avila and K. Moth-Poulsen, Single-molecule electronics: from chemical design to functional devices, *Chem. Soc. Rev.*, 2014, **43**, 7378–7411.
8 P. Gehring, J. M. Thijssen and H. S. van der Zant, Single-molecule quantum-transport phenomena in break junctions, *Nat. Rev. Phys.*, 2019, **1**, 381–396.
9 H. Oberhofer, K. Reuter and J. Blumberger, Charge transport in molecular materials: an assessment of computational methods, *Chem. Rev.*, 2017, **117**, 10319–10357.
10 G. Cohen and M. Galperin, Green's function methods for single molecule junctions, *J. Chem. Phys.*, 2020, **152**, 090901.
11 A. Jaroš, M. Sasar, L. Tučková, E. F. Bonab, Z. Badri, M. Straka and C. Foroutan-Nejad, Spinristor: A spin-filtering memristor, *Adv. Electron. Mater.*, 2023, **9**, 2300360.
12 M. O. Hight and T. A. Su, Opportunities in main group molecular electronics, *Trends Chem.*, 2024, **6**, 365–376.
13 Y. Tsuji, R. Hoffmann, M. Strange and G. C. Solomon, Close relation between quantum interference in molecular conductance and diradical existence, *Proc. Natl. Acad. Sci. U. S. A.*, 2016, **113**, E413–E419.
14 K. Kamada, K. Ohta, A. Shimizu, T. Kubo, R. Kishi, H. Takahashi, E. Botek, B. Champagne and M. Nakano, Singlet diradical character from experiment, *J. Phys. Chem. Lett.*, 2010, **1**, 937–940.
15 I. Fernández, *Aromaticity: Modern Computational Methods and Applications*, I. Fernández, Elsevier, 2021.
16 J. Kim, J. Oh, A. Osuka and D. Kim, Porphyrinoids, a unique platform for exploring excited-state aromaticity, *Chem. Soc. Rev.*, 2022, **51**, 268–292.
17 G. Merino, M. Solà, I. Fernández, C. Foroutan-Nejad, P. Lazzeretti, G. Frenking, H. L. Anderson, D. Sundholm, F. P. Cossío and M. A. Petrukhina, Aromaticity: Quo Vadis, *Chem. Sci.*, 2023, **14**, 5569–5576.
18 M. Solà, A. I. Boldyrev, M. K. Cyrański, T. M. Krygowski and G. Merino, *Aromaticity and Antiaromaticity*, John Wiley & Sons, Ltd, 2023, pp. 1–294.
19 M. Jirásek, H. L. Anderson and M. D. Peeks, From macrocycles to quantum rings: does aromaticity have a size limit?, *Acc. Chem. Res.*, 2021, **54**, 3241–3251.
20 J. Oh, Y. M. Sung, Y. Hong and D. Kim, Spectroscopic diagnosis of excited-state aromaticity: capturing electronic structures and conformations upon aromaticity reversal, *Acc. Chem. Res.*, 2018, **51**, 1349–1358.
21 T. Stuyver, S. Fias, F. De Proft, P. Geerlings, Y. Tsuji and R. Hoffmann, Enhancing the conductivity of molecular electronic devices, *J. Chem. Phys.*, 2017, **146**, 092310.

22 T. Stuyver, B. Chen, T. Zeng, P. Geerlings, F. De Proft and R. Hoffmann, Do diradicals behave like radicals?, *Chem. Rev.*, 2019, **119**, 11291–11351.
23 T. Stuyver, T. Zeng, Y. Tsuji, P. Geerlings and F. De Proft, Diradical character as a guiding principle for the insightful design of molecular nanowires with an increasing conductance with length, *Nano Lett.*, 2018, **18**, 7298–7304.
24 T. Stuyver, D. Danovich and S. Shaik, Captodative substitution enhances the diradical character of compounds, reduces aromaticity, and controls single-molecule conductivity patterns: A valence bond study, *J. Phys. Chem. A*, 2019, **123**, 7133–7141.
25 L. Li, C. R. Prindle, W. Shi, C. Nuckolls and L. Venkataraman, Radical single-molecule junctions, *J. Am. Chem. Soc.*, 2023, **145**, 18182–18204.
26 Y. Jiang, Y. Wang, P. Yang, H. Pan, Y. Wang, S. Sanvito and S. Hou, Origin of the reversed conductance decay in radical cationic molecular wires: a molecular orbital perspective, *J. Phys. Chem. C*, 2024, **128**, 21498–21507.
27 A. Sil, L. Hamilton, J. M. Morris, A. H. Daaoub, J. H. Burrows, C. M. Robertson, K. Luzyanin, S. J. Higgins, H. Sadeghi and R. J. Nichols, Zero-bias anti-ohmic behaviour in diradicaloid molecular wires, *Angew. Chem., Int. Ed.*, 2024, **63**, e202410304.
28 B. Lawson, E. Vidal Jr, S. Luna, M. M. Haley and M. Kamenetska, Extreme anomalous conductance enhancement in neutral diradical acene-like molecular junctions, *ACS Nano*, 2024, **18**, 29059–29066.
29 S. Gil-Guerrero, N. Ramos-Berdullas, Á. M. Pendás, E. Francisco and M. Mandado, Anti-ohmic single molecule electron transport: is it feasible?, *Nanoscale Adv.*, 2019, **1**, 1901–1913.
30 A. Bajaj and M. E. Ali, Anti-ohmic nanoconductors: myth, reality and promise, *Phys. Chem. Chem. Phys.*, 2023, **25**, 9607–9616.
31 S. Gil-Guerrero, Á. Peña-Gallego, N. Ramos-Berdullas, A. Martin Pendas and M. Mandado, Assessing the reversed exponential decay of the electrical conductance in molecular wires: the undeniable effect of static electron correlation, *Nano Lett.*, 2019, **19**, 7394–7399.
32 W. Chen, H. Li, J. R. Widawsky, C. Appayee, L. Venkataraman and R. Breslow, Aromaticity decreases single-molecule junction conductance, *J. Am. Chem. Soc.*, 2014, **136**, 918–920.
33 X. Yin, Y. Zang, L. Zhu, J. Z. Low, Z.-F. Liu, J. Cui, J. B. Neaton, L. Venkataraman and L. M. Campos, A reversible single-molecule switch based on activated antiaromaticity, *Sci. Adv.*, 2017, **3**, eaao2615.
34 A. Borges and G. C. Solomon, Effects of aromaticity and connectivity on the conductance of five-membered rings, *J. Phys. Chem. C*, 2017, **121**, 8272–8279.
35 T. Stuyver, M. Perrin, P. Geerlings, F. De Proft and M. Alonso, Conductance switching in expanded porphyrins through aromaticity and topology changes, *J. Am. Chem. Soc.*, 2018, **140**, 1313–1326.
36 Y. M. Sung, J. Oh, W.-Y. Cha, W. Kim, J. M. Lim, M.-C. Yoon and D. Kim, Control and switching of aromaticity in various all-aza-expanded porphyrins: spectroscopic and theoretical analyses, *Chem. Rev.*, 2017, **117**, 2257–2312.
37 T. Stuyver, S. Fias, P. Geerlings, F. De Proft and M. Alonso, Qualitative insights into the transport properties of Hückel/Möbius (anti)aromatic compounds: application to expanded porphyrins, *J. Phys. Chem. C*, 2018, **122**, 19842–19856.
38 S. M. Quintero, L. Van Nyvel, N. Roig, J. Casado and M. Alonso, Electron transport through linear-, broken-, and cross-conjugated polycyclic compounds, *J. Phys. Chem. A*, 2024, **128**, 6140–6157.
39 E. Desmedt, I. Casademont-Reig, R. Monreal-Corona, F. De Vleeschouwer and M. Alonso, Aromaticity in the spectroscopic spotlight of hexaphyrins, *Chem.–Eur. J.*, 2024, **30**, e202401933.
40 L. Leyva-Parra, R. Pino-Rios, D. Inostroza, M. Solà, M. Alonso and W. Tiznado, Aromaticity and magnetic behavior in benzenoids: unraveling ring current combinations, *Chem.–Eur. J.*, 2024, **30**, e202302415.
41 I. Casademont-Reig, T. Woller, V. García, J. Contreras-García, W. Tiznado, M. Torrent-Sucarrat, E. Matito and M. Alonso, Quest for the most aromatic pathway in charged expanded porphyrins, *Chem.–Eur. J.*, 2023, **29**, e202202264.
42 M. Alonso, P. Geerlings and F. De Proft, Exploring the structure-aromaticity relationship in Hückel and Möbius N-fused pentaphyrins using DFT, *Phys. Chem. Chem. Phys.*, 2014, **16**, 14396–14407.
43 M. Alonso, P. Geerlings and F. De Proft, Viability of Möbius Topologies in [26]- and [28]Hexaphyrins, *Chem.–Eur. J.*, 2012, **18**, 10916–10928.
44 I. Casademont-Reig, T. Woller, J. Contreras-García, M. Alonso, M. Torrent-Sucarrat and E. Matito, New electron delocalization tools to describe the aromaticity in porphyrinoids, *Phys. Chem. Chem. Phys.*, 2018, **20**, 2787–2796.
45 A. Mishra, C.-Q. Ma and P. Bauerle, Functional oligothiophenes: molecular design for multidimensional nanoarchitectures and their applications, *Chem. Rev.*, 2009, **109**, 1141–1276.
46 S. S. Zade, N. Zamoshchik and M. Bendikov, From short conjugated oligomers to conjugated polymers. Lessons from studies on long conjugated oligomers, *Acc. Chem. Res.*, 2011, **44**, 14–24.
47 R. Yamada, H. Kumazawa, T. Noutoshi, S. Tanaka and H. Tada, Electrical conductance of oligothiophene molecular wires, *Nano Lett.*, 2008, **8**, 1237–1240.
48 E. J. Dell, B. Capozzi, J. Xia, L. Venkataraman and L. M. Campos, Molecular length dictates the nature of charge carriers in single-molecule junctions of oxidized oligothiophenes, *Nat. Chem.*, 2015, **7**, 209–214.
49 Y. Zhang, S. Soni, T. L. Krijger, P. Gordiichuk, X. Qiu, G. Ye, H. T. Jonkman, A. Herrmann, K. Zojer and E. Zojer, Tunneling probability increases with distance in

junctions comprising self-assembled monolayers of oligothiophenes, *J. Am. Chem. Soc.*, 2018, **140**, 15048–15055.
50 Y. Ie, Y. Okamoto, T. Inoue, S. Tone, T. Seo, Y. Honda, S. Tanaka, S. K. Lee, T. Ohto and R. Yamada, Highly planar and completely insulated oligothiophenes: effects of π-conjugation on hopping charge transport, *J. Phys. Chem. Lett.*, 2019, **10**, 3197–3204.
51 C. E. Smith, S. O. Odoh, S. Ghosh, L. Gagliardi, C. J. Cramer and C. D. Frisbie, Length-dependent nanotransport and charge hopping bottlenecks in long thiophene-containing π-conjugated molecular wires, *J. Am. Chem. Soc.*, 2015, **137**, 15732–15741.
52 B. Capozzi, E. J. Dell, T. C. Berkelbach, D. R. Reichman, L. Venkataraman and L. M. Campos, Length-dependent conductance of oligothiophene, *J. Am. Chem. Soc.*, 2014, **136**, 10486–10492.
53 L. Xiang, T. Hines, J. L. Palma, X. Lu, V. Mujica, M. A. Ratner, G. Zhou and N. Tao, Non-exponential length dependence of conductance in iodide-terminated oligothiophene single-molecule tunneling junctions, *J. Am. Chem. Soc.*, 2016, **138**, 679–687.
54 T. Ohto, T. Inoue, H. Stewart, Y. Numai, Y. Aso, Y. Ie, R. Yamada and H. Tada, Effects of *cis-trans* conformation between thiophene rings on conductance of oligothiophenes, *J. Phys. Chem. Lett.*, 2019, **10**, 5292–5296.
55 T. Gao, C. He, C. Liu, Y. Fan, C. Zhao, C. Zhao, W. Su, Y. J. Dappe and L. Yang, Oligothiophene molecular wires at graphene-based molecular junctions, *Phys. Chem. Chem. Phys.*, 2021, **23**, 21163–21171.
56 T. Movlarooy, F. Enayati and R. Pilevarshahri, Molecular junction of n-thiophenes sandwiched between two Au (111) electrodes, *Mol. Phys.*, 2019, **117**, 6–10.
57 E. Leary, H. Höbenreich, S. J. Higgins, H. Van Zalinge, W. Haiss, R. J. Nichols, C. Finch, I. Grace, C. Lambert and R. McGrath, Single-molecule solvation-shell sensing, *Phys. Rev. Lett.*, 2009, **102**, 086801.
58 Y. Ie, M. Endou, S. K. Lee, R. Yamada, H. Tada and Y. Aso, Completely encapsulated oligothiophenes: synthesis, properties, and single-molecule conductance, *Angew. Chem.*, 2011, **123**, 12186–12190.
59 Y. Ie, M. Endou, A. Han, R. Yamada, H. Tada and Y. Aso, Functional oligothiophenes toward molecular wires in single-molecular electronics, *Pure Appl. Chem.*, 2012, **84**, 931–943.
60 S. K. Lee, R. Yamada, S. Tanaka, G. S. Chang, Y. Asai and H. Tada, Universal temperature crossover behavior of electrical conductance in a single oligothiophene molecular wire, *ACS Nano*, 2012, **6**, 5078–5082.
61 B. Q. Xu, X. L. Li, X. Y. Xiao, H. Sakaguchi and N. J. Tao, Electromechanical and conductance switching properties of single oligothiophene molecules, *Nano Lett.*, 2005, **5**, 1491–1495.
62 R. Ponce Ortiz, J. Casado, S. Rodriguez Gonzalez, V. Hernández, J. T. Lopez Navarrete, P. M. Viruela, E. Ortí, K. Takimiya and T. Otsubo, Quinoidal oligothiophenes: towards biradical ground-state species, *Chem.–Eur. J.*, 2010, **16**, 470–484.
63 P. M. Burrezo, J. L. Zafra, J. T. López Navarrete and J. Casado, Quinoidal/aromatic transformations in π-conjugated oligomers: vibrational Raman studies on the limits of rupture for π-bonds, *Angew. Chem., Int. Ed.*, 2017, **56**, 2250–2259.
64 Z. Zeng, X. Shi, C. Chi, J. T. L. Navarrete, J. Casado and J. Wu, Pro-aromatic and anti-aromatic π-conjugated molecules: an irresistible wish to be diradicals, *Chem. Soc. Rev.*, 2015, **44**, 6578–6596.
65 X. Ji and L. Fang, Quinoidal conjugated polymers with open-shell character, *Polym. Chem.*, 2021, **12**, 1347–1361.
66 J. Casado, R. P. Ortiz and J. T. L. Navarrete, Quinoidal oligothiophenes: new properties behind an unconventional electronic structure, *Chem. Soc. Rev.*, 2012, **41**, 5672–5686.
67 S. M. Quintero, J. L. Zafra, K. Yamamoto, Y. Aso, Y. Ie and J. Casado, Oligoene and cyanine features of tetracyano quinoidal oligothiophenes, *J. Mat. Chem. C*, 2021, **9**, 10727–10740.
68 G. Grover, J. D. Tovar and M. Kertesz, Quinonoid versus aromatic π-conjugated oligomers and polymers and their diradical characters, *J. Phys. Chem. C*, 2022, **126**, 5302–5310.
69 Y. Kim, Y.-J. Kim, Y.-A. Kim, E. Jung, Y. Mok, K. Kim, H. Hwang, J.-J. Park, M.-G. Kim and S. Mathur, Open-shell and closed-shell quinoid-aromatic conjugated polymers: unusual spin magnetic and high charge transport properties, *ACS Appl. Mater. Interfaces*, 2021, **13**, 2887–2898.
70 M. Kertesz, R. Bhattacharjee and J. D. Tovar, Quinonoid radial π-conjugation, *Chem. Sci.*, 2025, **16**, 14595–14604.
71 G. Grover, G. M. Peters, J. D. Tovar and M. Kertesz, Quinonoid vs. aromatic structures of heteroconjugated polymers from oligomer calculations, *Phys. Chem. Chem. Phys.*, 2020, **22**, 11431–11439.
72 R. Bhattacharjee and M. Kertesz, Topological Transition in Aromatic and Quinonoid π-Conjugated Polymers Induced by Static Strain, *J. Am. Chem. Soc.*, 2024, **146**, 26497–26504.
73 S. Ito, T. Suzuki, T. Kawai and T. Iyoda, Poly(benzo[c] thiophene-2-oxide) thin film, *Synth. Met.*, 2000, **114**, 235–242.
74 T. Takahashi, K.-i. Matsuoka, K. Takimiya, T. Otsubo and Y. Aso, Extensive quinoidal oligothiophenes with dicyanomethylene groups at terminal positions as highly amphoteric redox molecules, *J. Am. Chem. Soc.*, 2005, **127**, 8928–8929.
75 L. Zhang, N. S. Colella, B. P. Cherniawski, S. C. Mannsfeld and A. L. Briseno, Oligothiophene semiconductors: synthesis, characterization, and applications for organic devices, *ACS Appl. Mater. Interfaces*, 2014, **6**, 5327–5343.
76 R. van Asselt, I. Hoogmartens, D. Vanderzande, J. Gelan, P. E. Froehling, M. Aussems, O. Aagaard and R. Schellekens, New synthetic routes to poly (isothianaphthene) I. Reaction of phthalic anhydride and phthalide with phosphorus pentasulfide, *Synth. Met.*, 1995, **74**, 65–70.

77 M. Huskić, D. Vanderzande and J. Gelan, Synthesis of aza-analogues of poly(isothianaphthene), *Synth. Met.*, 1999, **99**, 143–147.
78 K. Lee and G. A. Sotzing, Poly(thieno [3,4-b] thiophene). A new stable low band gap conducting polymer, *Macromolecules*, 2001, **34**, 5746–5747.
79 B. Lee, M. S. Yavuz and G. A. Sotzing, Poly(thieno[3,4-*b*] thiophene)s from three symmetrical thieno[3,4-*b*] thiophene dimers, *Macromolecules*, 2006, **39**, 3118–3124.
80 R. Liu and Z. Liu, Polythiophene: Synthesis in aqueous medium and controllable morphology, *Sci. Bull.*, 2009, **54**, 2028–2032.
81 T. Yanai, D. P. Tew and N. C. Handy, A new hybrid exchange-correlation functional using the Coulomb-attenuating method (CAM-B3LYP), *Chem. Phys. Lett.*, 2004, **393**, 51–57.
82 M. J. Frisch, G. W. Trucks, H. B. Schlegel, G. E. Scuseria, M. A. Robb, J. R. Cheeseman, G. Scalmani, V. Barone, G. A. Petersson, H. Nakatsuji, X. Li, M. Caricato, A. V. Marenich, J. Bloino, B. G. Janesko, R. Gomperts, B. Mennucci, H. P. Hratchian, J. V. Ortiz, A. F. Izmaylov, J. L. Sonnenberg, D. Williams-Young, F. Ding, F. Lipparini, F. Egidi, J. Goings, B. Peng, A. Petrone, T. Henderson, D. Ranasinghe, V. G. Zakrzewski, J. Gao, N. Rega, G. Zheng, W. Liang, M. Hada, M. Ehara, K. Toyota, R. Fukuda, J. Hasegawa, M. Ishida, T. Nakajima, Y. Honda, O. Kitao, H. Nakai, T. Vreven, K. Throssell, J. A. Montgomery Jr, J. E. Peralta, F. Ogliaro, M. J. Bearpark, J. J. Heyd, E. N. Brothers, K. N. Kudin, V. N. Staroverov, T. A. Keith, R. Kobayashi, J. Normand, K. Raghavachari, A. P. Rendell, J. C. Burant, S. S. Iyengar, J. Tomasi, M. Cossi, J. M. Millam, M. Klene, C. Adamo, R. Cammi, J. W. Ochterski, R. L. Martin, K. Morokuma, O. Farkas, J. B. Foresman and D. J. Fox, *Gaussian 16 (Revision A.03)*, Gaussian Inc., Wallingford, CT, 2016.
83 T. H. Dunning Jr, Gaussian basis sets for use in correlated molecular calculations. I. The atoms boron through neon and hydrogen, *J. Chem. Phys.*, 1989, **90**, 1007–1023.
84 D. E. Woon and T. H. Dunning Jr, Gaussian basis sets for use in correlated molecular calculations. III. The atoms aluminium through argon, *J. Chem. Phys.*, 1993, **98**, 1358–1371.
85 B. Mahato and A. N. Panda, Assessing the performance of DFT functionals for excited-state properties of pyridine-thiophene oligomers, *J. Phys. Chem. A*, 2020, **125**, 115–125.
86 S. F. Parker, J. E. Trevelyan and H. Cavaye, Vibrational spectra of neutral and doped oligothiophenes and polythiophene, *RSC Adv.*, 2023, **13**, 5419–5427.
87 W. Michaels, Y. Zhao and J. Qin, Atomistic modeling of PEDOT: PSS complexes I: DFT benchmarking, *Macromolecules*, 2021, **54**, 3634–3646.
88 W. S. R. Jayasundara and G. Schreckenbach, Theoretical study of p-and n-doping of polythiophene-and polypyrrole-based conjugated polymers, *J. Phys. Chem. C*, 2020, **124**, 17528–17537.
89 A. D. Becke, Density-functional thermochemistry. III. The role of exact exchange, *J. Chem. Phys.*, 1993, **98**, 5648–5652.
90 C. Lee, W. Yang and R. G. Parr, Development of the Colle-Salvetti correlation-energy formula into a functional of the electron density, *Phys. Rev. B: Condens. Matter Mater. Phys.*, 1988, **37**, 785.
91 Y. Zhao and D. G. Truhlar, The M06 suite of density functionals for main group thermochemistry, thermochemical kinetics, noncovalent interactions, excited states, and transition elements: two new functionals and systematic testing of four M06-class functionals and 12 other functionals, *Theor. Chem. Acc.*, 2008, **120**, 215–241.
92 J. Pedersen and K. V. Mikkelsen, A benchmark study of aromaticity indexes for benzene, pyridine and the diazines-I. Ground state aromaticity, *RSC Adv.*, 2022, **12**, 2830–2842.
93 M. Vitek, J.-R. Deng, H. L. Anderson and I. Rončević, Global Aromatic ring currents in neutral porphyrin nanobelts, *ACS Nano*, 2024, **19**, 1405–1411.
94 D. W. Szczepanik, M. Sola, M. Andrzejak, B. Pawełek, J. Dominikowska, M. Kukułka, K. Dyduch, T. M. Krygowski and H. Szatylowicz, The role of the long-range exchange corrections in the description of electron delocalization in aromatic species, *J. Comput. Chem.*, 2017, **38**, 1640–1654.
95 L. Van Nyvel, M. Alonso and M. Solà, Effect of size, charge, and spin state on Hückel and Baird aromaticity in [*N*] annulenes, *Chem. Sci.*, 2025, **16**, 5613–5622.
96 J.-P. Malrieu and G. Trinquier, A recipe for geometry optimization of diradicalar singlet states from broken-symmetry calculations, *J. Phys. Chem. A*, 2012, **116**, 8226–8237.
97 C. F. Macrae, I. Sovago, S. J. Cottrell, P. T. Galek, P. McCabe, E. Pidcock, M. Platings, G. P. Shields, J. S. Stevens and M. Towler, Mercury 4.0: From visualization to analysis, design and prediction, *J. Appl. Crystallogr.*, 2020, **53**, 226–235.
98 M. Nakano, Electronic structure of open-shell singlet molecules: Diradical character viewpoint, *Top. Curr. Chem.*, 2017, **375**, 1–67.
99 K. Yamaguchi, The electronic structures of biradicals in the unrestricted Hartree-Fock approximation, *Chem. Phys. Lett.*, 1975, **33**, 330–335.
100 S. Ito and M. Nakano, Theoretical molecular design of heteroacenes for singlet fission: Tuning the diradical character by modifying π-conjugation length and aromaticity, *J. Phys. Chem. C*, 2015, **119**, 148–157.
101 I. Badía-Domínguez, S. Canola, V. Hernández Jolín, J. T. López Navarrete, J. C. Sancho-García, F. Negri and M. C. Ruiz Delgado, Tuning the diradical character of indolocarbazoles: impact of structural isomerism and substitution position, *J. Phys. Chem. Lett.*, 2022, **13**, 6003–6010.
102 M. Abe, Diradicals, *Chem. Rev.*, 2013, **113**, 7011–7088.
103 Ö. H. Omar, D. Padula and A. Troisi, Elucidating the relationship between multiradical character and predicted singlet fission activity, *ChemPhotoChem*, 2020, **4**, 5223–5229.

104 T. Minami and M. Nakano, Diradical character view of singlet fission, *J. Phys. Chem. Lett.*, 2012, **3**, 145–150.
105 C. Adamo and V. Barone, Toward reliable density functional methods without adjustable parameters: The PBE0 model, *J. Chem. Phys.*, 1999, **110**, 6158–6170.
106 E. Brémond and C. Adamo, Seeking for parameter-free double-hybrid functionals: The PBE0-DH model, *J. Chem. Phys.*, 2011, **135**, 024106.
107 B. O. Roos, P. R. Taylor and P. E. Sigbahn, A complete active space SCF method (CASSCF) using a density matrix formulated super-CI approach, *Chem. Phys.*, 1980, **48**, 157–173.
108 R. Ditchfield, W. J. Hehre and J. A. Pople, Self-consistent molecular-orbital methods. IX. An extended Gaussian-type basis for molecular-orbital studies of organic molecules, *J. Chem. Phys.*, 1971, **54**, 724–728.
109 W. J. Hehre, R. Ditchfield and J. A. Pople, Self—consistent molecular orbital methods. XII. Further extensions of Gaussian—type basis sets for use in molecular orbital studies of organic molecules, *J. Chem. Phys.*, 1972, **56**, 2257–2261.
110 P. C. Hariharan and J. A. Pople, The influence of polarization functions on molecular orbital hydrogenation energies, *Theor. Chim. Acta*, 1973, **28**, 213–222.
111 M. M. Francl, W. J. Pietro, W. J. Hehre, J. S. Binkley, M. S. Gordon, D. J. DeFrees and J. A. Pople, Self-consistent molecular orbital methods. XXIII. A polarization-type basis set for second-row elements, *J. Chem. Phys.*, 1982, **77**, 3654–3665.
112 C. S. López and O. N. Faza, Overview of the computational methods to assess aromaticity, in *Aromaticity*, I. Fernández, Elsevier, 2021, pp. 41–71.
113 R. Bader and M. Stephens, Fluctuation and correlation of electrons in molecular systems, *Chem. Phys. Lett.*, 1974, **26**, 445–449.
114 J. Poater, X. Fradera, M. Duran and M. Solà, The delocalization index as an electronic aromaticity criterion: application to a series of planar polycyclic aromatic hydrocarbons, *Chem.–Eur. J.*, 2003, **9**, 400–406.
115 J. Kruszewski and T. Krygowski, Definition of aromaticity basing on the harmonic oscillator model, *Tetrahedron Lett.*, 1972, **13**, 3839–3842.
116 E. Matito, M. Duran and M. Sola, The aromatic fluctuation index (FLU): A new aromaticity index based on electron delocalization, *J. Chem. Phys.*, 2005, **122**, 014109.
117 P. Bultinck, R. Ponec and S. Van Damme, Multicenter bond indices as a new measure of aromaticity in polycyclic aromatic hydrocarbons, *J. Phys. Org. Chem.*, 2005, **18**, 706–718.
118 M. Giambiagi, M. S. de Giambiagi and K. C. Mundim, Definition of a multicenter bond index, *Struct. Chem.*, 1990, **1**, 423–427.
119 M. Giambiagi, M. S. de Giambiagi, C. D. dos Santos Silva and A. P. de Figueiredo, Multicenter bond indices as a measure of aromaticity, *Phys. Chem. Chem. Phys.*, 2000, **2**, 3381–3392.
120 E. Matito, An electronic aromaticity index for large rings, *Phys. Chem. Chem. Phys.*, 2016, **18**, 11839–11846.
121 F. Feixas, E. Matito, J. Poater and M. Solà, On the performance of some aromaticity indices: a critical assessment using a test set, *J. Comput. Chem.*, 2008, **29**, 1543–1554.
122 M. Solà, F. Feixas, J. O. C. Jiménez-Halla, E. Matito and J. Poater, A critical assessment of the performance of magnetic and electronic indices of aromaticity, *Symmetry*, 2010, **2**, 1156–1179.
123 E. Matito, *ESI-3D: Electron Sharing Indices Program for 3D Molecular Space Partitioning*, Institute of Computational Chemistry and Catalysis (IQCC), University of Girona Catalonia, Spain, 2006.
124 T. A. Keith, *AIMAll, TK Gristmill Software: Overland Park, KS*, USA2019, vol. 23.
125 J. C. Cuevas and E. Scheer, *Molecular electronics: an introduction to theory and experiment*, World Scientific, 2010.
126 M. Naher, D. C. Milan, O. A. Al-Owaedi, I. J. Planje, S. Bock, J. Hurtado-Gallego, P. Bastante, Z. M. Abd Dawood, L. Rincón-García and G. Rubio-Bollinger, Molecular structure-(thermo)electric property relationships in single-molecule junctions and comparisons with single-and multiple-parameter models, *J. Am. Chem. Soc.*, 2021, **143**, 3817–3829.
127 J. P. Perdew, K. Burke and M. Ernzerhof, Generalized gradient approximation made simple, *Phys. Rev. Lett.*, 1996, **77**, 3865.
128 T. H. Dunning Jr and P. J. Hay, in *Methods of electronic structure theory*, H. F. Schaefer, Springer, 1977, vol. 3, pp. 1–27.
129 W. R. Wadt and P. J. Hay, Ab initio effective core potentials for molecular calculations. Potentials for main group elements Na to Bi, *J. Chem. Phys.*, 1985, **82**, 284–298.
130 M. Deffner, L. Groß, T. Steenbock, B. Voigt, G. Solomon and C. Herrmann, *Artaios-a code for postprocessing quantum chemical electronic structure calculations*, Universität Hamburg, 2010.
131 M. J. Frisch, G. W. Trucks, H. B. Schlegel, G. E. Scuseria, M. A. Robb, J. R. Cheeseman, G. Scalmani, V. Barone, G. A. Petersson, H. Nakatsuji, X. Li, M. Caricato, A. Marenich, J. Bloino, B. G. Janesko, R. Gomperts, B. Mennucci, H. P. Hratchian, J. V. Ortiz, A. F. Izmaylov, J. L. Sonnenberg, D. Williams-Young, F. Ding, F. Lipparini, F. Egidi, J. Goings, B. Peng, A. Petrone, T. Henderson, D. Ranasinghe, V. G. Zakrzewski, J. Gao, N. Rega, G. Zheng, W. Liang, M. Hada, M. Ehara, K. Toyota, R. Fukuda, J. Hasegawa, M. Ishida, T. Nakajima, Y. Honda, O. Kitao, H. Nakai, T. Vreven, K. Throssell, J. A. Montgomery Jr, F. Ogliaro, M. Bearpark, J. J. Heyd, E. Brothers, K. N. Kudin, V. N. Staroverov, T. Keith, R. Kobayashi, J. Normand, K. Raghavachari, A. Rendell, J. C. Burant, S. S. Iyengar, J. Tomasi, M. Cossi, J. M. Millam, M. Klene, C. Adamo, R. Cammi, J. W. Ochterski, R. L. Martin, K. Morokuma, O. Farkas,

J. B. Foresman and D. J. Fox, *Gaussian 09 (Revision D01)*, Gaussian, Inc., Wallingford CT, 2016.

132 E. Leary, A. La Rosa, M. T. González, G. Rubio-Bollinger, N. Agraït and N. Martín, Incorporating single molecules into electrical circuits. The role of the chemical anchoring group, *Chem. Soc. Rev.*, 2015, **44**, 920–942.

133 G. C. Solomon, C. Herrmann, T. Hansen, V. Mujica and M. A. Ratner, Exploring local currents in molecular junctions, *Nat. Chem.*, 2010, **2**, 223–228.

134 *Persistence of Vision Raytracer (Version 3.01)*. Persistence of Vision Pty. Ltd, Williamstown, Victoria, Australia, 2004.

135 K. Yamamoto, S. Jinnai, T. Takehara, T. Suzuki and Y. Ie, Quinoidal oligothiophenes having full benzene annelation: synthesis, properties, structures and acceptor application in organic photovoltaics, *Org. Lett.*, 2020, **22**, 547–551.

136 K. Yamamoto, S. Moles Quintero, S. Jinnai, E. Jeong, K. Matsuo, M. Suzuki, H. Yamada, J. Casado and Y. Ie, Cross-conjugated isothianaphthene quinoids: a versatile strategy for controlling electronic structures, *J. Mater. Chem. C*, 2022, **10**, 4421–4433.

137 K. Yamamoto, S. Jinnai and Y. Ie, Isothianaphthene quinoids: pyrazine-annelated structures for tunning electronic properties, *Bull. Chem. Soc. Jpn.*, 2024, **97**, uoae036.

138 L. V. Slipchenko and A. I. Krylov, Singlet–triplet gaps in diradicals by the spin-flip approach: A benchmark study, *J. Chem. Phys.*, 2002, **117**, 4694–4708.

139 A. Dreuw and M. Head-Gordon, Single-reference ab initio methods for the calculation of excited states of large molecules, *Chem. Rev.*, 2005, **105**, 4009–4037.

140 M. de Wergifosse, C. Bannwarth and S. Grimme, A simplified spin-flip time-dependent density functional theory approach for the electronic excitation spectra of very large diradicals, *J. Phys. Chem. A*, 2019, **123**, 5815–5825.

141 A. I. Krylov, Spin-flip equation-of-motion coupled-cluster electronic structure method for a description of excited states, bond breaking, diradicals, and triradicals, *Acc. Chem. Res.*, 2006, **39**, 83–91.

142 Y. Shao, M. Head-Gordon and A. I. Krylov, The spin-flip approach within time-dependent density functional theory: Theory and applications to diradicals, *J. Chem. Phys.*, 2003, **118**, 4807–4818.

143 Y. A. Bernard, Y. Shao and A. I. Krylov, General formulation of spin-flip time-dependent density functional theory using non-collinear kernels: Theory, implementation, and benchmarks, *J. Chem. Phys.*, 2012, **136**, 204103.

144 D. Casanova and A. I. Krylov, Spin-flip methods in quantum chemistry, *Phys. Chem. Chem. Phys.*, 2020, **22**, 4326–4342.

145 R. Gershoni-Poranne, A. P. Rahalkar and A. Stanger, The predictive power of aromaticity: quantitative correlation between aromaticity and ionization potentials and HOMO-LUMO gaps in oligomers of benzene, pyrrole, furan, and thiophene, *Phys. Chem. Chem. Phys.*, 2018, **20**, 14808–14817.

146 M. Kertesz, C. H. Choi and S. Yang, Conjugated polymers and aromaticity, *Chem. Rev.*, 2005, **105**, 3448–3481.

147 A. Bakhshi and J. Ladik, On the electronic properties of polyisothianaphthene, *Solid State Commun.*, 1987, **61**, 71–73.

148 J. Brédas, A. Heeger and F. Wudl, Towards organic polymers with very small intrinsic band gaps. I. Electronic structure of polyisothianaphthene and derivatives, *J. Chem. Phys.*, 1986, **85**, 4673–4678.

149 O. Kwon and M. L. McKee, Theoretical calculations of band gaps in the aromatic structures of polythieno[3,4-b] benzene and polythieno[3,4-b]pyrazine, *J. Phys. Chem. A*, 2000, **104**, 7106–7112.

150 I. Casademont-Reig, E. Ramos-Cordoba, M. Torrent-Sucarrat and E. Matito, *Aromaticity descriptors based on electron delocalization in Aromaticity*, I. Fernández, Elsevier, 2021, pp. 235–259.

151 Y. S. Lee and M. Kertesz, The effect of additional fused rings on the stabilities and the band gaps of heteroconjugated polymers, *I. J. Quantum Chem.*, 1987, **32**, 163–170.

152 F. Feixas, E. Matito, J. Poater and M. Solà, Quantifying with electron delocalisation measures, *Chem. Soc. Rev.*, 2015, **44**, 6424–6451.

153 F. De Vleeschouwer, E. Desmedt and M. Alonso, Exploting aromaticity in expanded porphyrins: a multidimensional approach to structure-property relationships, *Chem. Meth.*, 2025, 202500064.